UTRECHT UNIVERSITY

Institute for Marine and Atmospheric Research Utrecht (IMAU)

Master Thesis in Climate Physics

A study on mesoscale eddies in the Irminger Sea and Iceland Basin using high resolution mooring data and satellite altimetry

by Lisa Novak

First examiner:
Dr. C.E. (Claudia) Wieners

Second examiner:
Prof. dr. ir. H.A. (Henk) Dijkstra

In cooperation with:
Dr. M. Femke de Jong
Nora Fried
Royal Netherlands Institute for Sea Research (NIOZ)

July 3, 2023

Abstract

The Irminger Sea and Iceland Basin are the main regions of deep water formation which feed the lower limb of the Atlantic Meridional Overturning Circulation (AMOC). This deep water formation occurs due to deep convection in winter and restratification in summer. Changes in stratification have far-reaching effects on the deep water formation, ultimately impacting the climate of western Europe and the North Atlantic region. Ocean eddies transport different water masses through the entire ocean outside of large scale circulations. They have the potential to transport buoyant water to the convection region, therefore impacting restratification. In this study we use six years of high resolution mooring observations in the Irminger Sea to determine the vertical and horizontal structures, temperature and salinity of anticyclonic eddies. Additionally, we employ a global dataset of eddies tracked through satellite altimetry to analyze the horizontal structures and propagation of eddies across the eastern subpolar North Atlantic. Twelve eddies have been detected through mooring observations. We find that eddies at the mooring reach depths of up to 850 m with salinity between 35.02 g kg^{-1} and 35.15 g kg^{-1} and temperatures between 5.0° and 6.6°C. The radii of mooring detected eddies lie between 16.5 km and 33.1 km. Based on our analysis of globally tracked eddies using satellite altimetry, we observe no discernible distinction in the characteristics of anticyclonic eddies between the Irminger Sea and Iceland Basin in a mean over a 30-year period. The tracked eddies have a mean radius of 34 km and a mean lifetime of 60 days. They mainly travel westward over the span of their lifetime. Eddy propagation is influenced by strong currents and shallow topography, but independent of the background flow in the basin interior. The findings in this study enhance our understanding of the characteristics and dynamics of anticyclonic eddies in the Irminger Sea and Iceland Basin. The insights gained from this research need yet to be linked to stratification and convection.

Contents

1 Introduction

Ocean eddies are important features to the ocean system. They redistribute heat and salt and transport biological and chemical components (Pegliasco, Busché, and Faugère, 2022). Eddies are large drivers of mesoscale variability, as they contribute to stratification in the ocean (Sterl and de Jong, 2022; Danek et al., 2023) and furthermore can influence not only marine life but also large scale ocean circulations (Raj et al., 2016). Though the knowledge of eddies is already quite extensive, there is still a lack of in-depth knowledge of the characteristics of eddies in the Irminger Sea and Iceland Basin. This study aims to provide detailed information on the horizontal and vertical structures, the lifetimes and propagation of anticyclonic eddies in this region.

The Atlantic Meridional Overturning Circulation (AMOC) is a thermo-haline circulation that transports warm and saline water to the North in the upper Atlantic (upper AMOC limb) and colder, fresher water to the South in the deep Atlantic (lower limb). Due to the northward heat transport the AMOC plays an important role in the North Atlantic and European climate (Weaver et al., 2007; Delworth and Zeng, 2012; Jackson et al., 2022). Over the next century many models project the AMOC to decline. While models agree on a decline of the AMOC, the magnitude remains uncertain due to limited observations and modeling limitations (IPCC, 2021). It is therefore an important and interesting ocean feature to research.

Due to the potential impacts on the climate system, marine biogeochemistry and the cryosphere through changes in the Overturning circulation initiatives have been taken to better understand the AMOC variability and its consequences (Lozier et al., 2017). To increase long-term and in-situ observations, in 2014 the Overturning in the subpolar North Atlantic Program (OSNAP) has been installed, which comprises moorings, floats, and gliders, deployed and maintained by various international research institutes. OSNAP provides continuous recordings of heat, volume, and freshwater fluxes and velocities in the entire water column across the array, facilitating comprehensive monitoring (https://www.o-snap.org/; Li, Lozier, Holliday, et al., 2021; Lozier et al., 2017; Li, Lozier, Bacon, et al., 2021).

As part of the subpolar North Atlantic, the Irminger Sea and Iceland Basin, have

become focus of more attention in recent years, particularly the Irminger Sea. The Irminger Sea lies East of Greenland, and ranges from the Greenland coast to the Reykjanes Ridge (RR), which extends South-West from Iceland. The Iceland Basin is East of the RR and south of Iceland, as depicted in Figure 1. It has been discovered that the Iceland Basin and Irminger Sea have a greater impact on deep water formation, supplying the lower limb of the AMOC, contrary to the previous belief that the Labrador Sea was the primary contributor (Marzocchi et al., 2015; Petit et al., 2020; Jackson et al., 2022). Li, Lozier, Bacon, et al., 2021 found that most of the variability in the overturning stems from the Eastern side of the OSNAP array.

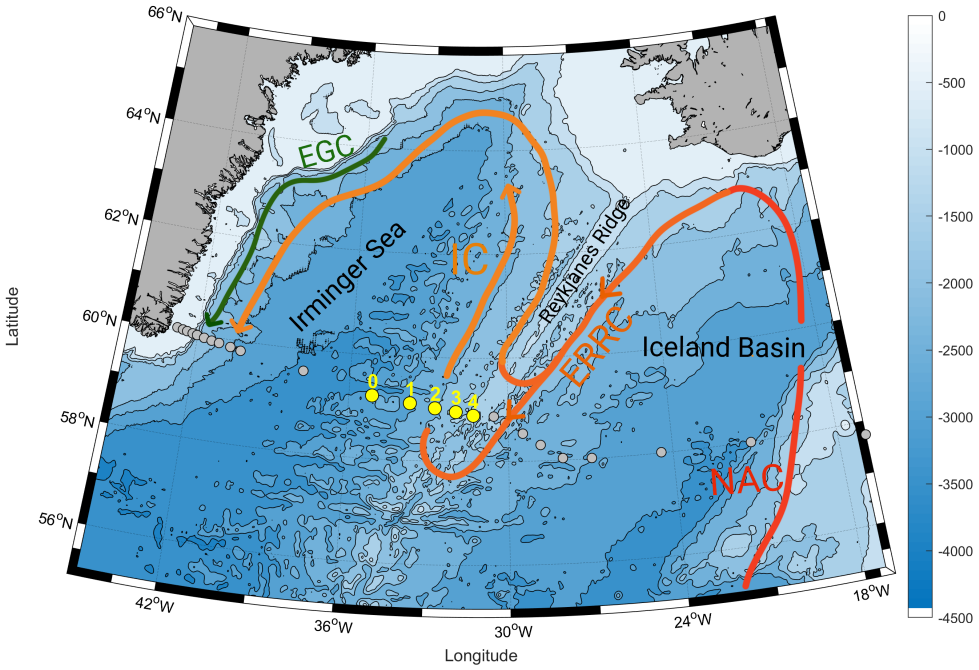

Figure 1: Schematic of the Irminger Sea with bottom topography. Yellow dots show the location of the NIOZ array moorings (IC0 - IC4) west of the Reykjanes Ridge (RR). Gray dots show the observations sites of the OSNAP array. The depicted currents are the North Atlantic Current (NAC), East Reykjanes Ridge Current (ERRC), Irminger Current (IC) and East Greenland Current (EGC).

Figure 1 shows the studied region and a schematic of the currents. The North

Atlantic Current (NAC) transports warm and saline water northward into the Irminger Sea and Iceland Basin. On the eastern flank of the RR, the East Reykjanes Ridge Current (ERRC) returns this water southward and crosses the Reykjanes Ridge. On the western flank of the Reykjanes Ridge, the North Atlantic Current and the ERRC turn into the Irminger Current (IC), which flows West of the (RR) and further transports the warm, saline water to around 65°, where it turns westward, and flows towards Greenland, turning further, and then moves southward, creating a surface cyclonic gyre. (Higginson et al., 2011; Fan et al., 2013; Josey et al., 2019; de Jong et al., 2020). The East Greenland Current (EGC), which transports colder denser water southward, is the colder flank of the IC on the western side of the Irminger Sea (Krauss and Kase, 1998; Våge et al., 2011).

As part of the OSNAP array, the Royal Netherlands Institute for Sea Research (NIOZ) has installed five moorings on the western flank of the RR, located in the central Irminger Current. The moorings are called IC0, IC1, IC2, IC3 and IC4, going from West to East. The mooring locations are indicated in Figures 1 and 2. The IC consists of two surface intensified cores that transport the warm saline water southward (de Jong et al., 2020). Figures 2a to 2d show the mean fields of V , U (velocity components perpendicular to and along the OSNAP array respectively), absolute salinity (S) and conservative temperature (Θ) from 2014 - 2020. In Figure 2a the two core system can be seen, with the western core located around IC1, and the eastern core located around IC3 and IC4. The salinity and temperature mean fields (Figures 2c , 2d) show that the Irminger Sea becomes warmer and more saline towards the East.

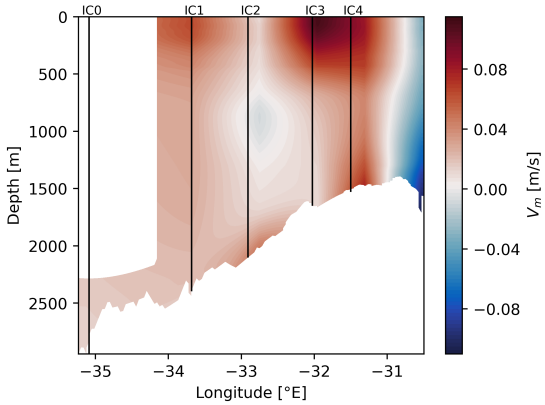

(a) Mean across array velocity (v_m) from mooring observations 2014 - 2020

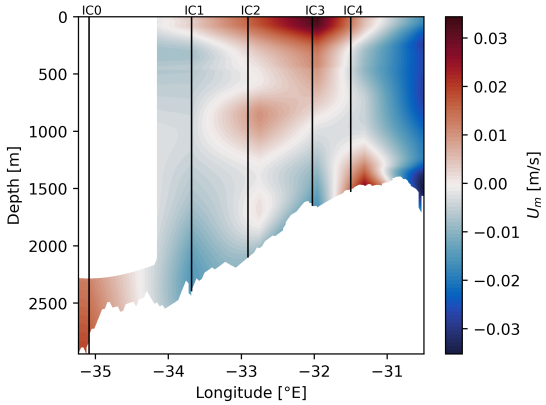

(b) Mean along array velocity (u_m) from mooring observations 2014 - 2020

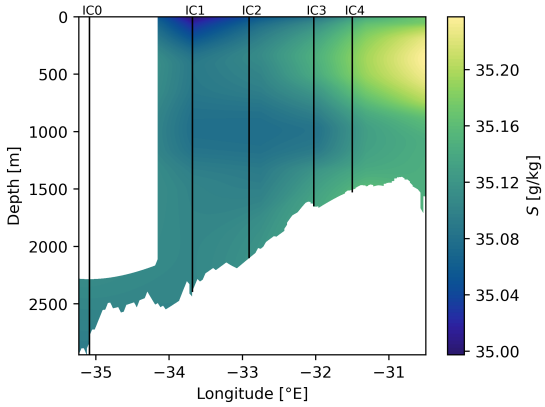

(c) Mean salinity from mooring observations 2014 - 2020

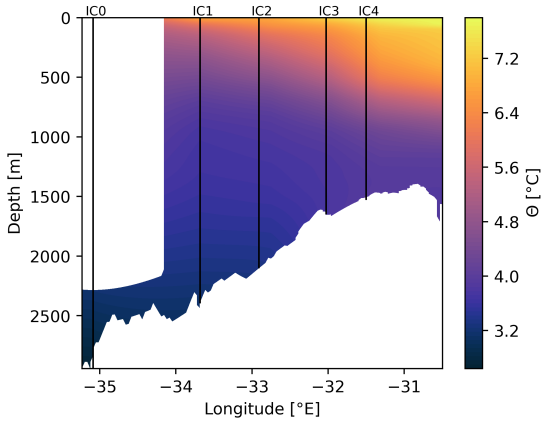

(d) Mean conservative temperature from mooring observations 2014 - 2020

Figure 2: 6-year mean of mooring observations with the locations of the moorings indicated as black lines. IC0 is a short mooring, that ends 2240m below the surface, therefore there is no data in the upper water column.

Eddies are usually seen as anomalous compared to the ocean background, because they are generated through instabilities of currents (Pegliasco, Delepoulle, et al., 2022). Eddies like these are found in the form of anticyclones in the Labrador Sea, where near Cape Farewell, the southernmost tip of Greenland, the returning Irminger Current sheds off warm and saline vortices, called Irminger Rings (de Jong et al., 2014). Eddies are also generated through wind induced instabilities or due to topographic changes (Pegliasco, Delepoulle, et al., 2022). In the Labrador Sea and Irminger Sea anticyclonic eddies are a source of buoyant, salty and warm water (Lilly and Rhines, 2002; Fan et al., 2013). Especially anticyclonic

eddies have therefore been studied in the high-latitude North-Atlantic, where they are a prominent feature. They have been studied in these regions with in-situ and satellite altimetry measurements and show similar characteristics (Lilly and Rhines, 2002; Fan et al., 2013; de Jong et al., 2014; Raj et al., 2016; Sandalyuk et al., 2020).

The Irminger Sea and Iceland Basin largely contribute to the overturning in the subpolar North Atlantic, which occurs due to deep convection in winter and re-stratification in summer. In winter, as the surface temperature cools down, the top layer of the water becomes more dense than the lower layer. The dense water moves downward, mixing with the lower layers. If the surface cooling continues, the mixing also continues, thus leading to an increase in mixed layer depth and loss of stratification. In this process the dense, cold water that feeds the lower limb of the AMOC is formed. In summer, as the surface temperature increases again, the water column is restratified. Anticyclonic eddies carry warm and buoyant water to the Irminger Sea, and therefore contribute to restratification (Sterl and de Jong, 2022). It is therefore important to study (anticyclonic) eddy activity in the Irminger Sea.

Fan et al., 2013 have studied anticyclonic eddies in the Irminger Sea between 2002 - 2009 using mooring and glider observations. While this gives insight in the vertical structure, and estimates of the horizontal structure of eddies, there is still limited knowledge. Recent studies in the Iceland Basin on anticyclonic eddies exist (Zhao et al., 2018; Kondetharayil Soman et al., 2022), but are limited to eddies with lifetimes of more than four weeks. This research aims to address the following questions:
Quantification: What is the total number of eddies present in the studied region?
Propagation of eddies: What are the overall lifetime paths of these eddies, both in a larger temporal context and on a daily basis? How strongly is the movement of eddies influenced by the background flow?
Structural characteristics: What are the horizontal and vertical structures and how high are salinity and temperature of eddies
Comparative evaluation of datasets: How effectively do different datasets perform to analyze eddies?
This study utilizes five moorings, deployed by NIOZ, in the central path of the IC.

With mooring observations the vertical structure, the salinity and temperature of eddies is analyzed. Satellite altimetry data and a collection of globally tracked eddies dating back to 1993 are used to quantify the horizontal structures and eddy activity in the Irminger Sea and Iceland Basin. The goal is to compare and assess these datasets to gain a comprehensive understanding of eddy dynamics in the Irminger Sea and Iceland Basin.

This paper is structured as follows: Section 2 introduces the datasets used for this study. Section 3 explains the methods used. Section 4 presents the results found and Section 5 gives the conclusions of the findings of this study and an outlook on further research.

2 Data

2.1 Mooring Timeseries

2.1.1 Instrumentation

As part of the OSNAP array NIOZ has installed five moorings West of the RR. The observations of the moorings are composed of four deployments, two 1-year and two 2-year deployments (2014-2015, 2015-2016, 2016- 2018 and 2018-2020), they have last been serviced and redeployed in July 2022 (de Jong et al., 2020; Fried and de Jong, 2022). The installation of the NIOZ mooring array is up-to-date; however, for the purpose of this analysis, a time frame of six years, spanning from July 2014 to July 2020, has been considered.

Four of the NIOZ array moorings monitor the entire water column (IC1, IC2, IC3 and IC4) and reach from 45 m below the surface to the bottom between 2494 m (IC1) and 1471 m (IC4). The four tall moorings are placed in the main path of the IC. IC0 is a short mooring, reaching from 2939 m to 2240 m and is installed to study overflow waters (de Jong et al., 2020). The eddies detected by mooring observations in this study are surface eddies with a maximum depth of 850 m. Observations from the short mooring are therefore not considered. The mooring observations have a temporal resolution of one day. Mesoscale eddies have lifespans of days to years. Fan et al., 2013 studies mesoscale anticyclonic eddies in the Irminger Sea with mooring data of higher resolution (20 min), and found a mean lifetime of 10 days and radii between 4 km and 21 km . The temporal and vertical resolution of the NIOZ moorings are therefore expected to be high enough to detect similar eddies, and derive their vertical structures and estimates of their radius.

The velocities are measured with single-point current meters at 728 m and 980 m using Aanderaa RCM11 and at 1428 m, 2234 m and 2467 m depth using Nortek Aquadopps with a sampling rate of 30 min. At the target depth of 475 m upward looking Acoustic Doppler Current Profilers (ADCPs) (RDI 75 kHz Long Ranger ADCPs) are installed, measuring velocities up to 50m at a sampling rate of 1 h.

Temperature, pressure and conductivity are measured with Sea-Bird Electronics SBE37 (MicroCATs) at a sampling rate of 15 min and are located at approximately

55 m, 430 m, 980 m, 1485 m and 2480 m depth. Sea-Bird Electronics SBE56 (thermistors) additionally measure temperature every 5 min at approximately 190 m and 390 m depth.

2.1.2 Mooring Data Processing

To remove tides and inertial motions the velocity data is low-pass filtered by a 41-hr sixth-order Butterworth filter. It is then subsampled onto a daily grid. The velocities are furthermore rotated clockwise by 10°. This is done in order to have a velocity component that is parallel (u_m) and a component perpendicular (v_m) to the OSNAP Array. Using MATLAB's "pchip" function, the data is vertically interpolated between the instruments. In the horizontal the data is linearly interpolated between the moorings, following bottom contours. More information on the mooring data and processing can be found in de Jong et al., 2020 and Fried and de Jong, 2022.

2.2 Altimetry Data

Additionally altimetry data is used to compare to mooring observations and detect eddies using sea level anomaly. Anticyclonic eddies have a positive SLA and therefore can be detected using either sea level anomaly or absolute dynamic topography. The "Global Ocean Gridded L4 Sea Surface Heights And Derived Variables Reprocessed 1993 Ongoing" from E.U. Copernicus Marine Service Information (https://doi.org/10.48670/moi-00148) is a dataset containing various variables derived from all altimeter Copernicus missions (Sentinel-6A, Sentinel-3A/B) and other collaborative or opportunity missions (e.g. :Jason- 3, Saral[-DP]/AltiKa, Cryosat-2, OSTM/Jason2, Jason-1, Topex/Poseidon, Envisat, GFO, ERS-1/2, Haiyang-2A/B). The L 4 product is a gridded altimeter product with a spatial coverage ranging from latitudes -90° to 90° and longitudes from -180° to 180°. It has a spatial resolution of 0.25°x0.25° and a daily temporal resolution extending from 01-01-1993 to 31-12-2020. The dataset contains a variety of variables derived from sea surface height (SSH). For this study we use sea level anomaly (SLA), absolute dynamic topography (ADT), as well as the geostrophic velocities in zonal and meridional direction.

2.3 Global Mesoscale Eddy Trajectory Atlas

Eddies cannot only be seen in altimetry data, but SLA and ADT can be used to track eddies over their lifetime. The Global Mesoscale Eddy Trajectory Atlas enables us to adress the question of the amount of eddies, their overall lifetime, their horizontal structure and their propagation. The altimetric Mesoscale Eddy Trajectory Atlas product (META3.2 DT allsat, DOI: https://10.24400/527896/a01-2022.005.220209; (Pegliasco et al., 2022)) was produced by SSALTO/DUACS and distributed by AVISO+ (www.aviso.altimetry.fr) with support from CNES, in collaboration with IMEDEA. This atlas was downloaded the 22 March 2023, and covers the period from January 1993 to Febuary 2022. The eddies are divided into six groups. Anticyclonic and cyclonic eddies, long tracked eddies (longer than 10 days), short tracked eddies (strictly shorter than 10 days) and untracked eddies.

This product uses gridded global absolute dynamic topographies from Copernicus Marine Service (CMEMS, https://marine.copernicus.eu/) to find and track eddies. A full description of the eddy tracking algorithm can be found in (Pegliasco, Delepoulle, et al., 2022). The algorithm is derived from (Mason et al., 2014). Table 1 contains the variables used in this study.

Table 1: Variables contained in the altimetric Mesoscale Eddy Trajectory Atlas product (META3.2 DT allsat)

Variable	Description
Latitude and Longitude	Center of eddy
Effective contour	Contour of outer edges
Speed contour	Contour of highest velocity
Effective radius	Radius of best fit circle to effective contour
Speed radius	Radius of best fit circle to speed contour
Effective area	Area enclosed by effective contour
Amplitude	Magnitude of height difference between the SSH extremum within eddy and SSH around effective contour
Time	Date of observation
Track	Trajectory identification number

3 Methods

This section explains the methods used for this study. Section 3.1 discusses the methodology used to detect eddies and derive their propagation velocity, translation direction and radius from mooring data. Sections 3.2 and 3.3 explain how the altimetry data and eddy trajectory atlas are used to gain additional information about eddies in the Irminger Sea and Iceland Basin. The altimetry data and eddy trajectory atlas provide a wide range of variables (see also Section 2), and thus, additional methodologies are not extensively necessary. By conducting these additional comparisons and assessments, a comprehensive understanding of the relationships and discrepancies between various datasets is achieved, enhancing the overall interpretation of the study results.

3.1 Eddy Detection from Mooring Observations

Anticyclones are vortices with a warm, saline core and less dense water compared to the surrounding water in the Irminger Sea. If the core of an eddy passes by a mooring it can be detected through increase in temperature and salinity and the measured velocity signals. Depending on the propagation direction and distance of the eddy core to the mooring, an eddy leaves distinct velocity signatures (discussed in depth further down). Figure 3 shows an example of an eddy passing by a mooring. In the beginning of December 2019 salinity and temperature are higher than in the surrounding time frame. During this period a downward displacement of isopycnals is observed as well. Both velocities show a change of direction, though it is more prominent in the v component (velocity v_m - top panel of figure 3).

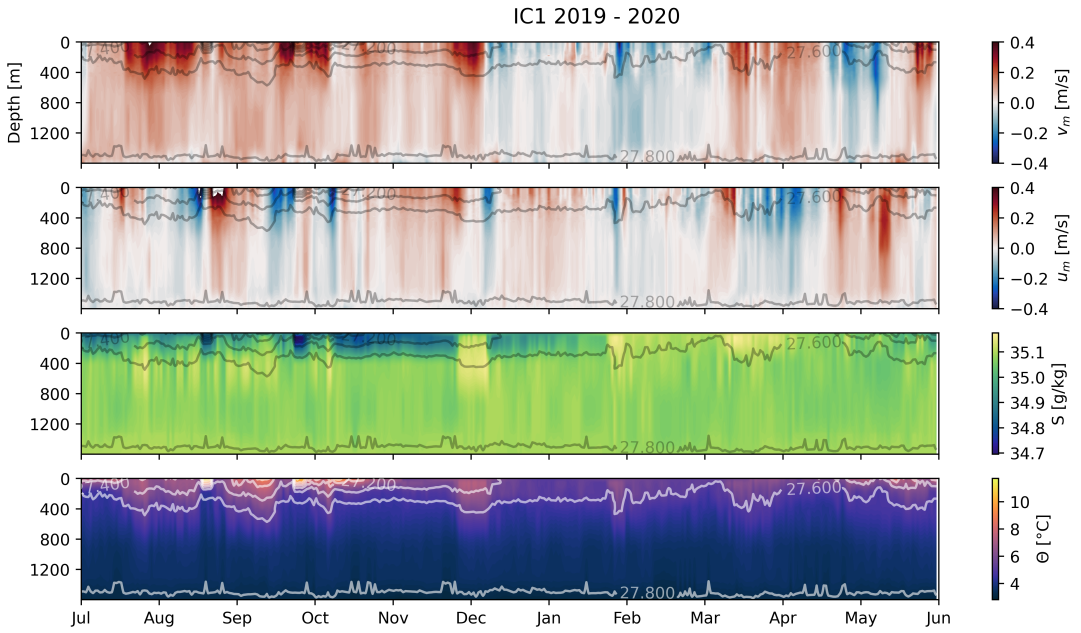

Figure 3: One-year time series of IC1. Top panel shows velocity v_m (v rotated 10°). Second panel from the top shows velocity u_m (u rotated 10°). Third panel shows absolute salinity and bottom panel shows conservative temperature, all panels include isopycnals.

Due to seasonal cycles in hydographic properties and because anticyclones consist of anomalous water, a more effective way of detecting eddies is by using an anomaly time series. The anomaly time series is derived by subtracting a three-month mean around each month. This time frame is chosen to remove seasonal cycles. Figure 4 shows the anomaly time series of the same time frame as figure 3. Note that the isopycnals are still given in absolute values, not anomalies. The eddy already seen in the time series of absolute values becomes even more prominent in the anomaly time series, showing a strong positive anomaly in Θ and S that reaches to around 800 m depth, with a weaker, but still positive anomaly below 800 m.

A visual skimming of the data is not sufficient to conclusively determine whether an eddy like event is indeed an eddy. To detect eddies from mooring time series similar techniques as in Lilly and Rhines, 2002; Fan et al., 2013 and de Jong et al., 2014 are followed here.

Salinity and Temperature Signals

In a first step events of high salinity and temperature are determined. The anomaly

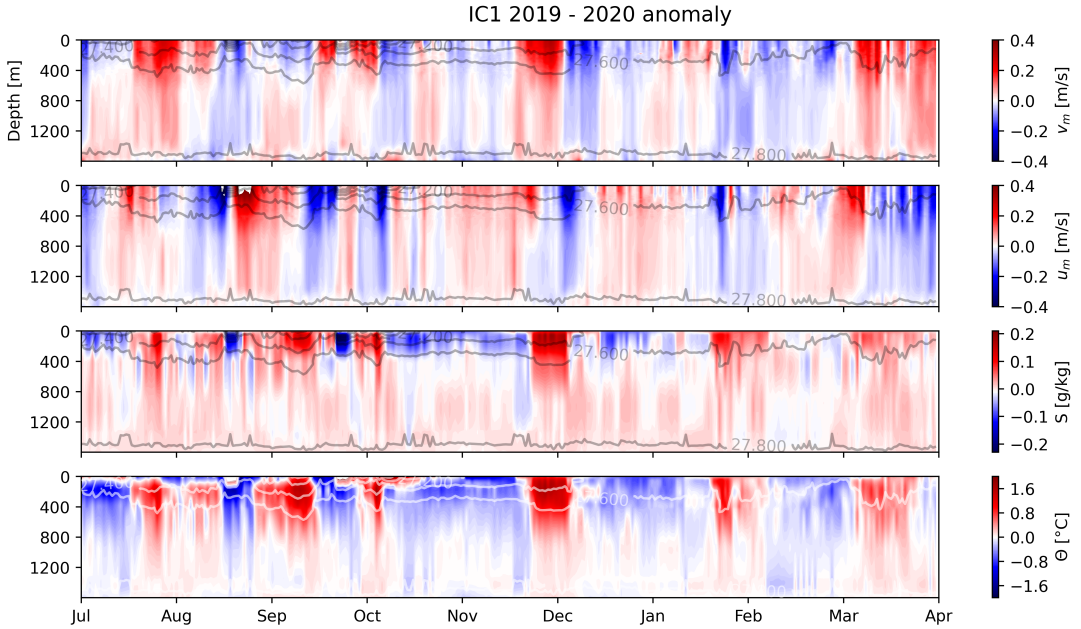

Figure 4: One-year anomaly time series of IC1. Anomalies are derived by subtracting a three-month running mean. Top panel shows velocity v_m (v rotated 10°). Second panel from the top shows velocity u_m (u rotated 10°). Third panel shows absolute salinity and bottom panel shows conservative temperature anomalies, all panels include isopycnals.

time series of all moorings show that anomalies of eddy-like events reach a depth of at least 450 m. We therefore compare the daily means of the top 450 m to the annual 800 m mean. The depth of 800 m is chosen, because the lower parts of the ocean are colder and less involved in mixing and therefore experience less changes in temperature and salinity. This can be seen in Figure 4, where there are minimal changes below 800 m. An anomaly is counted as significant if the daily mean over the top 450 m of salinity and temperature exceeds one standard deviation of the annual mean over the top 800 m.

Density and Velocity Signals

We then proceed to look at corresponding changes in density and velocity of the detected salinity and temperature anomalies. Due to more buoyant water that anticyclonic eddies carry to the Irminger Sea, isopycnals are displaced downwards. For velocity changes there are multiple scenarios to consider. It is common practice to estimate ocean eddies with a Rankine vortex (see also Lilly and Rhines, 2002 and de Jong et al., 2014). In a Rankine eddy the azimuthal velocity is given by

$$v_c = \begin{cases} \frac{Vr}{R}, & r < R \\ \frac{VR}{r}, & r > R \end{cases} \tag{1}$$

In the ideal Rankine velocity signal, the center of the eddy is the point where both velocities are 0, as there is no azimuthal movement in the center. The eddy core is the region between the azimuthal velocity maxima. In an ideal eddy this is a circle, where the velocities are highest at the edge of the circle. The circle corresponds to the eddy core and the edges of the circle are the edges of the eddy core. To describe the measured velocity signals when an eddy crosses by a mooring consider Figure 5, which shows two different "mooring tracks". The mooring track is the line the mooring leaves on the eddy, as it passes over the mooring. If the center of an eddy crosses the mooring directly (red line through circle), one velocity component remains quasi constant. This velocity component is parallel to the mooring track (called the along velocity, v_a). The other velocity component is perpendicular to the mooring track (the cross velocity v_c) and follows the azimuthal velocity of Eq. (1). This is depicted in Figure 5, where the peaks of the velocity are aligned with the edge of the eddy core (highest velocity). The blue line through the circle shows an alternative eddy track, where the center does not cross the mooring. In this case both velocity components exhibit changes. The distance between the peaks of the cross velocity indicate how many days it takes the eddy core to cross the mooring. Half their distance is therefore an indication of the radius of the eddy core with the unit days.

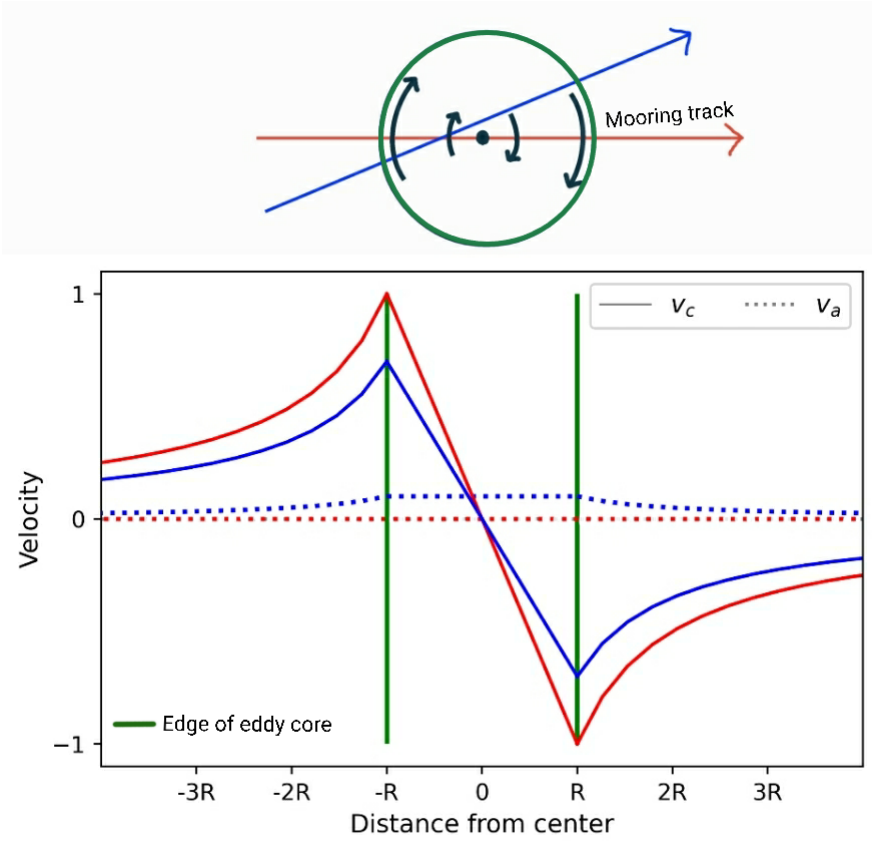

Figure 5: Velocity profile of ideal Rankine eddy. v_c is the cross velocity, the component perpendicular to the mooring track. v_a the along velocity, the component parallel to the mooring track. Vertical green lines indicate the edges of the eddy core (highest velocities).

In an eddy the velocities are surface intensified, therefore, the velocity signals here have been derived from the daily mean over the top 250 m. Very few eddies cross the mooring with the center, but are more likely to cross the mooring with their core or outer edge. If the core crosses, both velocity components will exhibit changes (see Figure 5). In this case the velocities are rotated such that the cross array velocity component u_m best fits the azimuthal velocity of the Rankine eddy $u_{m,rot} = v_c$, and is therefore perpendicular to the mooring track. The other component is near constant $v_{m,rot} = v_a$, and rotated such that it is aligned with the mooring track. Figure 7 shows the velocity signals rotated to best fit a Rankine eddy for an eddy crossing IC1 in November 2014. If the eddy core does not cross the mooring and the mooring only catches the outer edges, the velocity signals will likely not be strong enough to derive any further properties. Figure 6 shows an example of an eddy observed by IC1 in May 2019. The top panel shows the

daily 250 m mean of the velocities, and the density line, the lower panel shows the daily 450 m mean of salinity and temperature as well as the annual 800 m mean and standard deviation thereof.

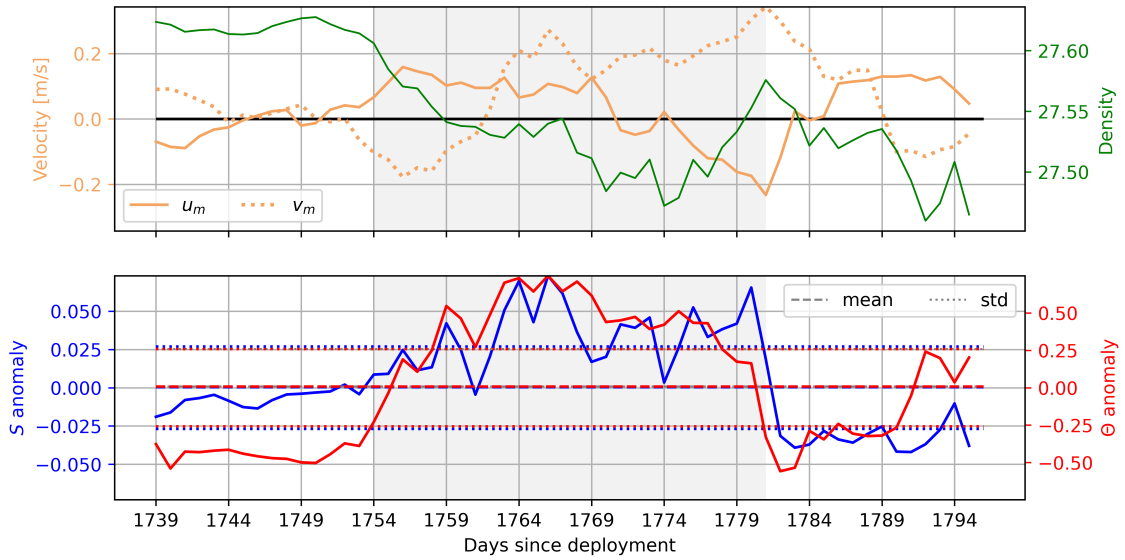

Figure 6: Velocity, temperature and salinity profile of an eddy crossing over IC1 in May 2019.

If all above mentioned requirements are fulfilled an event is considered an eddy. Due to high variability at the mooring site, especially in the velocity component, automatic detection of eddies proves difficult, which other studies have also found (e.g. de Jong et al., 2014).

Deriving further properties of eddies from mooring data

If an event is identified as an eddy further properties describing the eddy can be obtained from the mooring data. These properties include the duration of salinity and temperature anomalies, salinity and temperature of the eddy core, the radius, travel direction and propagation velocity.

The rotation angle with which the velocity field is rotated is the travel direction of the eddy. The mooring velocity observations are composed of the azimuthal velocity of the eddy, and the propagation velocity. The propagation velocity can be extracted through the following procedure: With velocities of $0.3\,\mathrm{m\,s^{-1}}$ and length scales of 30 km, the Rossby number is small enough to assume geostrophic balance, and therefore the cross velocity can further be estimated using sea level

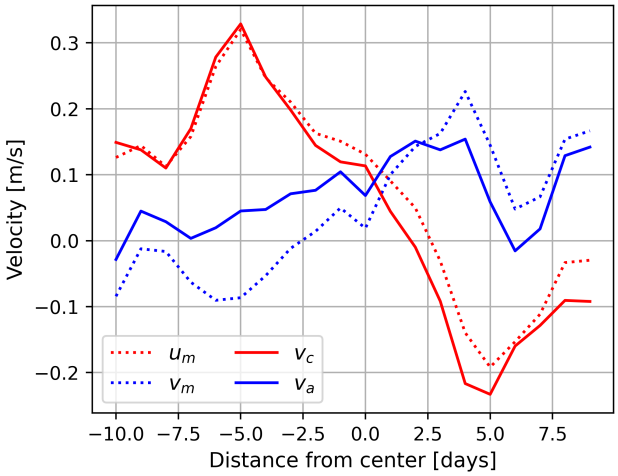

Figure 7: Velocity signals during eddy like event in November 2014 at IC1. Dotted lines are the mooring velocities, solid lines are the velocities rotated by 34.38°, such that u_m is perpendicular to the mooring track and best fits the rankine eddy velocity. The apparent radius is 5 days.

height gradients. The geostophic balance can be written as

$$v_c = \frac{g}{f}\frac{d\eta}{dx} \tag{2}$$

with f and g the Coriolis parameter and gravitational acceleration respectively and η the sea level anomaly. We now approximate the length scale $dx \approx U_{prop} \cdot dt$, where U_{prop} is the propagation velocity of the eddy traveling past the mooring. Assuming that $\eta \approx D$, where D is the dynamic height, the approximation for the cross velocity becomes

$$v_c \approx \frac{g}{f}\frac{dD}{U_{prop}dt} \tag{3}$$

where dx is the eddy radius in m, and dt is the apparent eddy radius in days (derived from the velocity signals). The dynamic height D is calculated with the Gibbs Sea Water (gsw) library for python, from salinity, temperature and pressure. By fitting eq (3) to the cross velocity from the rotated velocity field of an eddy occurrence, the propagation velocity can be determined. A more robust es-

timate of the propagation velocity is obtained by performing two fits to the data, on either side of the edge of the eddy core: one around the maximum (2 days before and after the maximum) and one around the minimum (2 days before and after the minimum). The outcome is more robust because it is possible for the propagation velocity to vary over time, especially for eddies that are near the mooring over a longer timespan (more than 15 days). We now assume the propagation velocity to vary linearly between the two outcomes. The radius can be calculated using $dx = U_{prop} \cdot dt$ with dt the apparent radius. Figure 8 shows an example of the fit procedure for an eddy that was observed in January 2015.

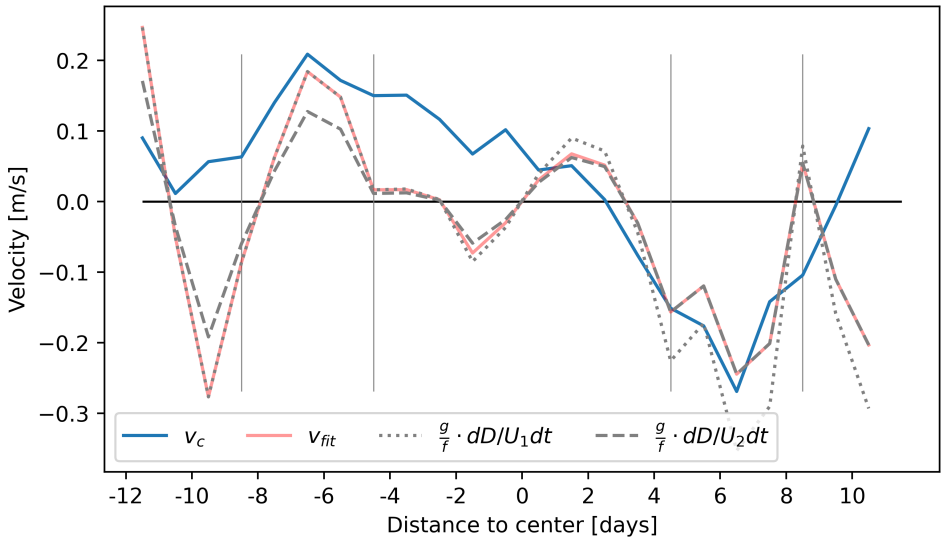

Figure 8: Example of fit to cross velocity to determine propagation velocity and consequently the radius of an eddy (Eddy 4, January 2015). Vertical lines indicate region where fits are performed. The gray lines (dotted and dashed) are the fits performed around the maximum and minimum respectively. The red line is the resulting fit, assuming U_{prop} to vary linearly.

3.2 Altimetry Data

The mooring observations are used to verify the accuracy of the altimetry data and eddy trajectory atlas. Anticyclonic eddies have a slightly elevated sea surface. In altimetry data they can therefore be detected by circular positive anomalies in sea level. The Global Mesoscale Eddy Trajectory Atlas bases the eddy detection on absolute dynamic topography (ADT). To compare the tracked eddies to altimetry data the ADT provided by Copernicus Marine Service Information is used. Similarly to the mooring data, the ADT anomaly is derived by subtracting

a three-month mean. The tracked eddy dataset does not provide the ADT used to detect and track eddies. ADT anomaly presented in this paper may therefore differ slightly, but suffices for the purposes of this study. Furthermore, this study includes a comparison between SLA from altimetry data at the mooring location and the dynamic height anomaly derived from the mooring data specifically during the presence of observed eddies. This analysis allows for an evaluation of the agreement between altimetry data and mooring observations within the context of the detected eddies. Additionally, the translation direction obtained from the mooring eddies can be compared to the movement of the eddy as observed in the altimetry data.

3.3 Global Mesoscale Eddy Trajectory Atlas

An important component of this study involves examining whether the eddies observed by the mooring are also identified and tracked within the global mesoscale eddy trajectory atlas, and furthermore gain insights into the characteristics of eddies in the Irminger Sea and Iceland Basin with nearly 30 years of tracked eddies.

Division into coherent subregions

In order to efficiently analyze the extensive dataset encompassing 30 years of tracked eddies, an approach has been adopted whereby the selected region has been subdivided into smaller, more coherent segments based on the underlying bottom topography or background flow. The Irminger Sea and Iceland Basin are further divided into the following regions, as seen in Figure 9. A1 and A2 are small regions located West and East of the Reykjanes Ridge. B is situated south of Iceland and functions as a control region due to the observable pattern of travel direction of eddies. Region D encloses a region around IC1, the mooring primarily used for eddy detection from mooring observations. Region C is a large region in the Iceland Basin, that excludes strong bottom topography. Region E is the equivalent in the Irminger Sea. All properties are extracted for each region separately.

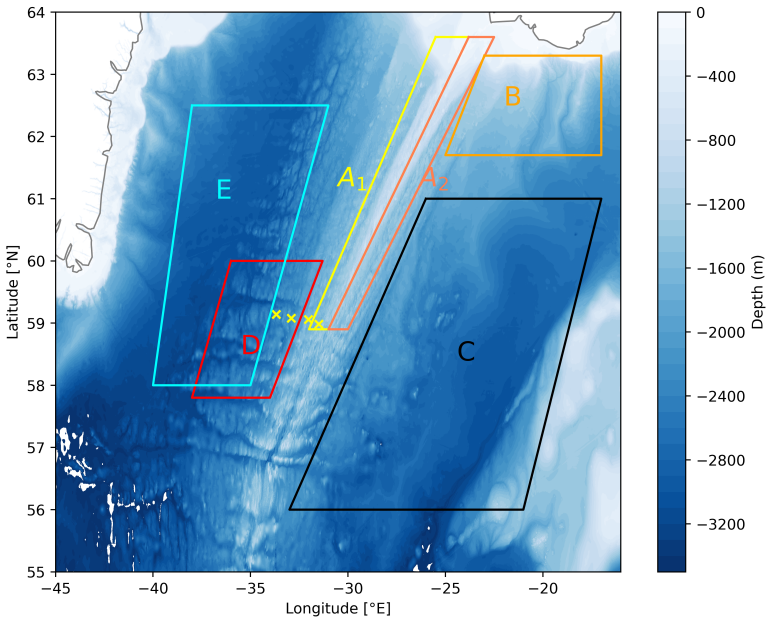

Figure 9: Division of Irminger Sea and Iceland Basin into smaller coherent regions.

Translation direction

For more insight into the horizontal behavior of eddies, the translation direction of eddies is derived by calculating the direction from the first tracked day to the last tracked day of an eddy. Instances where eddies exhibit different directions on certain days or remain relatively stationary for some time, are therefore not captured. For region D the translation directions are compared to the findings of mooring observations.

Influence of background flow on eddy propagation

To examine the influence of background flow on eddy propagation, the geostrophic velocities derived from altimetry data are analyzed. The mean velocity values are computed for the period of 1993-2022 within a 0.25x0.25 grid, corresponding to the dataset's resolution. At each grid point the velocity between two consecutive entries of a tracked eddy are determined, thus creating a grid of the same resolution the mean eddy propagation.

An example of a full analysis of an eddy can be found in the Appendix. The example is of eddy 6 in September 2018, because while it demonstrates the methods used, it also shows the variability of the data and the resulting limitations in the methods.

4 Results

This section presents the results found in this study. First the results from applying the methods discussed in Section 3.1 in the mooring data are presented. In Section 4.2 we examine the alignment of the altimetry data with the mooring observations, assessing whether they provide consistent findings. This comparison allows us to evaluate the reliability and agreement between the datasets. In Section 4.3 we also start with assessing the consistency between the tracked eddy dataset and the mooring observations. Following that, we present additional findings derived from the eddy trajectory atlas. These findings extend beyond the comparison with mooring observations and provide further insights into the eddy activity in the Irminger Sea and Iceland Basin.

4.1 Eddies detected by mooring observations

IC1 recorded 53 occurrences of salinity and temperature threshold crossings. IC2 recorded 59, IC3 recorded 62 and IC4 recorded 49. Automatic extraction of eddy properties beyond the threshold crossing of temperature and salinity is not reliable due to the high variability in the velocity signals on which further analysis is based. Due to time constraints, the focus of this study lies on the eddies detected by IC1 and the eddy trajectory atlas, instead of the other moorings, allowing a more comprehensive examination of eddies over a wider region. IC1 is chosen due to higher eddy kinetic energy here, and is therefore expected to have more eddies close to it.

Out of the 53 threshold crossings in IC1, 12 occurrences have been identified as eddies. Their properties can be found in Table 2. The eddies are numbered in chronological order of their appearance. The salinity of the eddies lies between $35.02\,\mathrm{g\,kg^{-1}}$ and $35.15\,\mathrm{g\,kg^{-1}}$. The temperature values lie between 5.0° and 6.6°. Salinity, temperature and duration of the eddies vary with no systematic changes in the six years of observed eddies. The amount of standard deviations above the mean of the eddies' salinity threshold increases slightly over the six years, indicating that the Irminger Sea has become less saline - an observation also found by mooring data and other studies (Holliday et al., 2020). The observed eddies predominantly travel northward, with a majority displaying a north-westward

trajectory. Only two of the observed eddies move southward. The mooring lies in the western core of the Irminger Current which has a mean northward flow and therefore the eddies seem to follow the IC. This is further analyzed in Section 4.3. The radii are expected to lie between 15 km and 45 km in the Irminger Sea (see also results in Lilly and Rhines, 2002; Fan et al., 2013; de Jong et al., 2014), and between 31 km and 91 km in the Iceland Basin (Zhao et al., 2018; Kondetharayil Soman et al., 2022). The mean radius of the observed eddies is 22.7 km. This mean excludes the radii of two eddies, as they lie far above the expected range (eddies 3 with 122 km and 9 with 69 km). The propagation velocities of the detected eddies range from 0.7 cm s^{-1} and 11.4 cm s^{-1}, though only three eddies have higher propagation velocities than 4.5 cm s^{-1}, which is the highest velocity measured by the mooring. The depths of the eddy cores vary between 450 m and 850 m. Figure 10 shows the vertical profile of salinity and temperature of the center of Eddy 7 in May 2019. In the center the salinity anomaly extends to around 900 m and the temperature is higher than the mean over the entire depth.

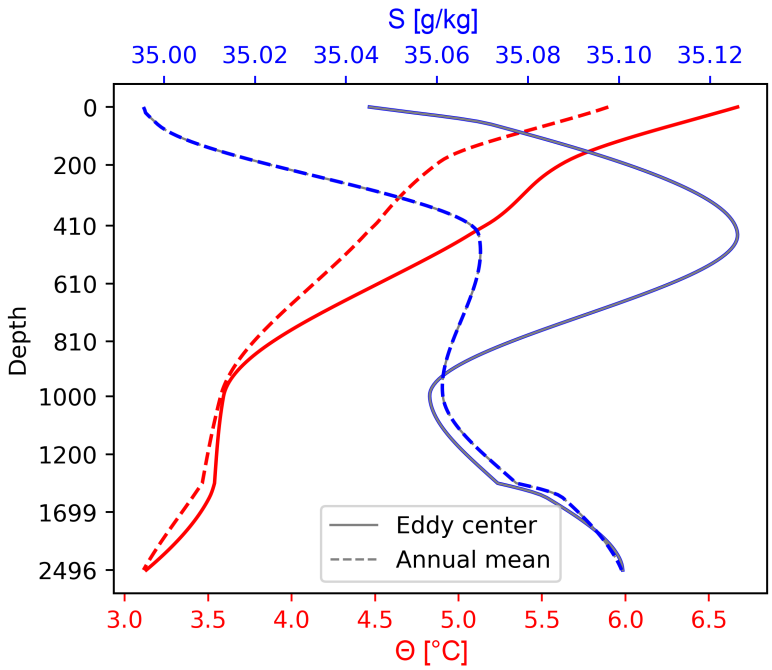

Figure 10: Vertical temperature and salinity profile of eddy center. Eddy 7 in May 2019. Depicted is also the annual mean.

Shortcomings of method to derive U_{prop} and the radius

The mean radius of 22.7 km lies within the expected range, however, the method

used to extract the propagation velocity from the mooring observations and consequently the radius, shows noteworthy shortcomings. Fitting the geostrophic balance to the cross velocity is done on either side of the eddy core in order to get two estimates of the propagation velocity. For some observed velocity signals this works well, resulting in an overall accurate fit where the two estimates for the propagation velocity only differ slightly (see Figure 8). For other eddies the difference in propagation velocity and consequently radius varies strongly for either side of the eddy core. Figures 11a and 11b show examples of this. Here the resulting fit (v_{fit}) is accurate. However, there is a significant variation in U_{prop} between the two edges of the eddy core. Consequently, this discrepancy leads to two estimates of the radius that differ significantly from each other, with one of the radii lying far outside the expected range. Eddies 3 and 9 stand out due to their high radii, which lie significantly outside the expected range. These eddies also deviate from the typical size range observed in the dataset, suggesting an anomalous behavior or potentially erroneous derivation of the propagation velocity and radius. These eddies do not only stand out due to their high radii, but also show significantly higher propagation velocities than the other eddies, which also helps explain the high radii. In addition eddy 3 has an apparent radius of 18 days, which is twice as high as the mean (9 days). This long duration of the anomaly contributes to the large estimate of the radius. Overall 7 out of the 12 detected eddies give robust results for the propagation velocity and radius.

With the applied methods 12 eddies have been detected by IC1, and the properties have been derived from the observations. Unlike other studies on eddies detected by mooring data (Fan et al., 2013; de Jong et al., 2014) the NIOZ array moorings are not located in an ideal place for eddy detection. The extraction of properties through these moorings is therefore more erroneous, but the eddies show properties expected for this region.

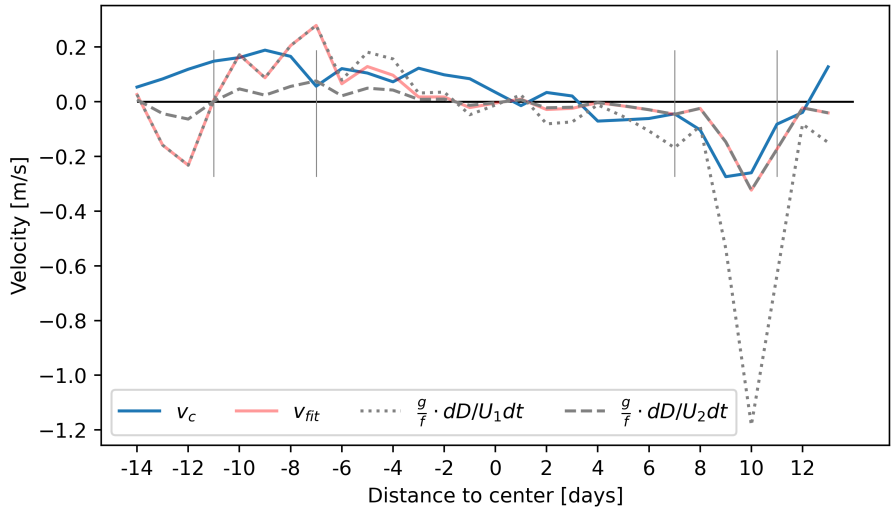

(a) Eddy 1, December 2014. Resulting radii from fitting either side of the eddy core: 20 km and 73 km.

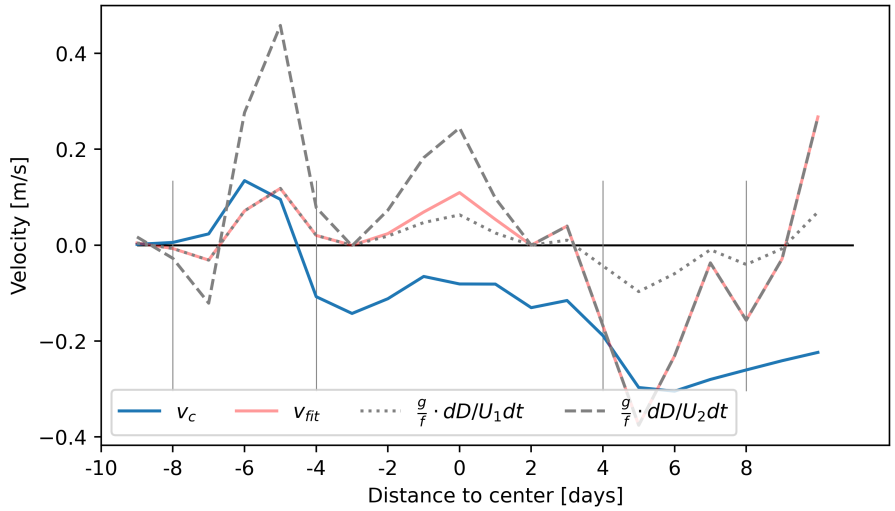

(b) Eddy 8, August 2019. Resulting radii from fitting either side of the eddy core: 311 km and 33 km

Figure 11: Estimation of propagation velocity by fitting dynamic height gradient to the cross velocity v_c. Dotted line presents the fit using the first peak of v_c, dashed line using the second peak (first and second time the eddy core edges cross the mooring).

Table 2: Properties of eddies derived from mooring data. The numbers in brackets in column 2 and 3 indicate the amount by which the S and Θ anomalies lie above the threshold in std.

Eddy	S [g/kg]	Θ [°C]	Depth [m]	Anomaly duration	Translation direction ° from N	U_{prop} [cm/s]	Radius [km]
0 Nov 14	35.1439 (0.9)	6.56 (0.4)	450	12	23	4.5	17.36
1 Dec 14	35.1509 (0.6)	6.07 (0.9)	600	20	17	2.6	20.12
2 Jan 15	35.1497 (0.5)	5.58 (1.1)	700	12	107	3.9	27.12
3 Oct 15	35.1074 (2.6)	5.61 (1.6)	700	36	43	11.4	172.38
4 Dec 15	35.1273 (0.6)	5.00 (0.1)	800	13	351	3.3	18.32
5 Dec 17	35.0752 (2.8)	5.41 (1.8)	850	20	32	3.5	17.98
6 Sep 18	35.0198 (0.4)	6.39 (1.9)	450	29	3	4.1	26.63
7 May 19	35.0698 (1.3)	5.05 (1.3)	850	27	52	3.1	33.14
8 Aug 19	35.0729 (2.6)	5.39 (1.3)	850	10	40	0.7	30.76
9 Sep 19	35.0669 (1.6)	5.73 (1.8)	800	25	23	5.5	68.82
10 Dec 19	35.1205 (3.3)	5.74 (2.0)	800	15	318	2.7	16.48
11 Mar 20	35.1065 (1.5)	5.03 (1.1)	800	14	191	8.8	19.03

4.2 Mooring detected eddies in altimetry data

Twelve eddies have been found in the mooring data. The analysis of eddy properties from mooring data shows limitations and uncertainties. To further analyze eddies in the Irminger Sea and Iceland Basin we use altimetry data. For this we consider SLA during occurrences of an eddy detected by the mooring. Anticyclonic eddies show a positive SLA, and 11 out of 12 eddies show a positive circular anomaly traveling close to IC1. Figure 12a shows the 2019-09-21, where a circular positive anomaly is seen close to IC1. During this time eddy 6 was observed by mooring data. For most eddies the SLA anomaly signals are not as clear. See for example Figure 12b. Here The area East of IC1 is shows positive SLA, with two circular anomalies close to the mooring. Without further analysis, it is not clear which eddy the mooring caught. To determine which eddy is caught by the mooring the global mesoscale eddy trajectory atlas provides further information.

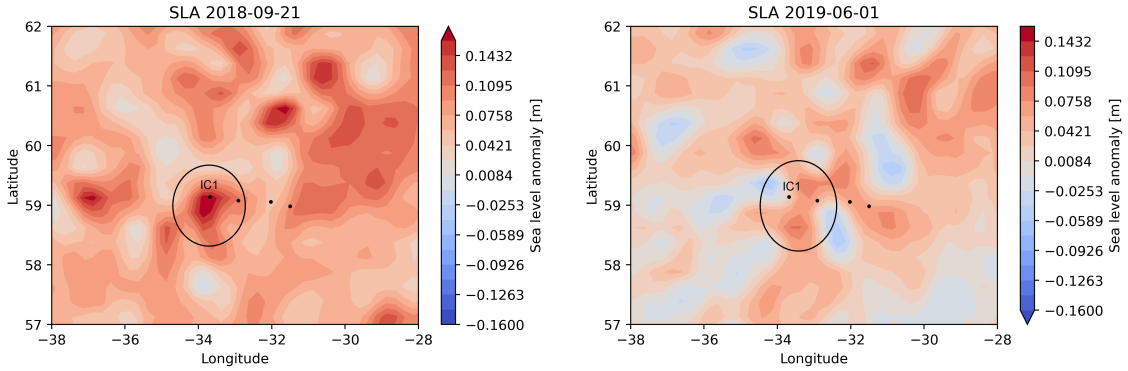

(a) sla during eddy 6 (Sept 2018). Black dots indicate mooring positions.

(b) sla anomaly during eddy 7 (May 2019). Two circular anomalies are close to IC1.

Figure 12

Further comparison can be done by comparing the SLA at the mooring (from altimetry data) to the calculated dynamic height anomaly (mooring data). This comparison is insightful, because the method used to determine the propagation velocity and radius of eddies from mooring observations approximates sea level anomaly with dynamic height anomaly (see Section 3.1). For some eddies SLA and dynamic height anomaly coincide very well. Figure 13a shows an example of this. For most eddies however the mooring observations and altimetry data differ significantly. An example of this is shown in Figure 13b. There is no cor-

relation between agreement of dynamic height anomaly derived by mooring observations with satellite SLA and robust estimates of the radius derived through mooring data. The examples in Figure 13 show eddy 1, with agreement between the datasets, however the analysis of eddy 1 from mooring data does not yield reliable and conclusive results, as discussed in Section 4.1. Conversely, for eddy 10, which produces robust results in the mooring analysis, SLA and dynamic height anomaly do not align, as illustrated in Figure 13b. Overall, there is limited agreement between altimetry SLA and mooring dynamic height anomaly, highlighting the challenges and discrepancies in capturing the characteristics of these eddies. The altimetry data is limited in temporal and spacial resolution, and is therefore highly interpolated.

The travel direction of the eddies seen in altimetry data coincide with the findings of mooring analysis. Of the 11 eddies seen in SLA all travel to the North.

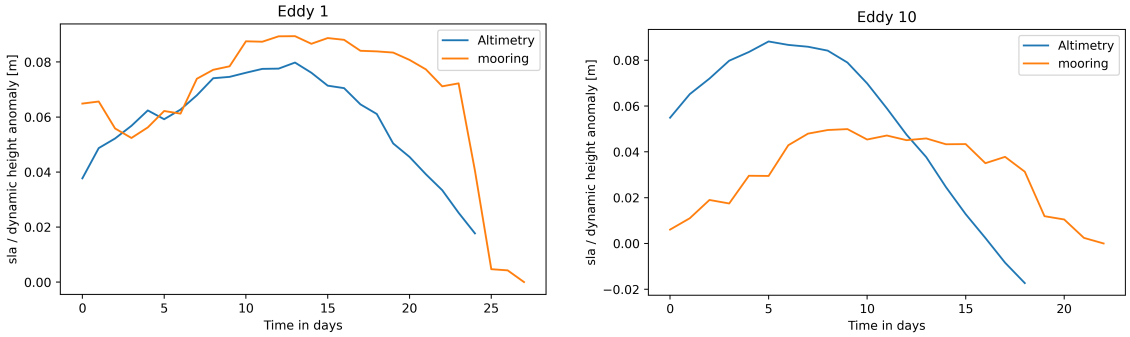

(a) Eddy 1 (Nov 2014).

(b) Eddy 10 (Dec 2019).

Figure 13: SLA (altimetry) and dynamic height anomaly (mooring) data comparison

4.3 Tracked eddies in Irminger Sea and Iceland Basin

The mesoscale eddy trajectory atlas contains tracked eddies globally. For the purposes of this study the region between 55°N and 63°N and 318°W and 341°W is considered.

4.3.1 Mooring detected eddies in mesoscale eddy trajectory atlas

Eleven out of twelve eddies found in the mooring are also present in the tracked eddy dataset. Ten of these are long tracked eddies (> 10 days), and one is an eddy shorter than ten days. Between 2014 and 2020, the time frame of the mooring observations, 43 eddies are tracked within the range of where other eddies have been detected by the mooring. This means only 26% of tracked eddies near IC1 are detected in mooring observations, indicating that 34 tracked eddies go undetected. Among these undetected tracked eddies, 11 directly pass over the mooring. Considering the limitations imposed by the low temporal and spatial resolution of altimetry data, which necessitates extensive interpolation, the location of the tracked eddy centers is only an approximation. Consequently, there is a possibility that tracked eddies, which appear to be passing by the mooring based on their projected locations, were not close enough to be detected in mooring observations. To further investigate why many tracked eddies go undetected in mooring observations we have looked at the mooring data during the time eddies were tracked near the mooring, specifically we have looked at the 11 tracked eddies that seem to pass directly by the mooring. Out of these, seven do not cross the salinity and temperature threshold and are therefore not considered in the mooring observations. The remaining four satisfy the salinity and temperature requirements but do not have the necessary velocity signal, density signal, or both to continue with further analysis. The mooring observations give insights in the vertical structure of the detected eddies, as well as the properties of the transported water masses. Due to high background variability in the velocity at the mooring site, many eddies are missed by the mooring and extraction of their properties is not possible. As other studies have shown (Fan et al., 2013; de Jong et al., 2014) eddies in the subpolar North Atlantic are similar to each other, a conclusion also found by the mooring data in this study. The eddy trajectory

atlas contains 11 out of 12 eddies caught by the mooring and many more and can therefore be used to gain further information on the mesoscale eddy activity in the Irminger Sea and Iceland Basin.

4.3.2 Tracked Eddies in the Irminger Sea and Icelandic Basin

In total the global mesoscale trajectory atlas records 10 362 anticyclonic eddies longer than 10 days and 6174 strictly shorter than 10 days in the Irminger Sea and Icelandic Basin between 1993 and 2022. The specific number of eddies per region (see Section 3.3 and Figure 9 for the regions) is provided in Table 3. The numbers are divided into eddies that cross a region and eddies that originate in a region. The results show that there are more long lived eddies than short ones. The regions A1 and A2 (around RR) both have a similar size and a similar amount of eddies. With a tendency to travel towards the West (discussed in Section 4.3.3), there are fewer eddies that originate on the eastern flank of the RR. Regions D (around IC1) and B (South of Iceland) are similar in size and have similar amount of eddies. Regions C (Iceland Basin) and E (Irminger Sea) are the largest regions and have most eddies.

Table 3: Number of tracked eddies per region, divided into eddies that cross a region and eddies that originate in a region. Amount of short eddies are eddies that cross the region.

Region	Crossing	Originating	Short
A1	759	489	340
A2	598	299	228
B	728	700	278
C	2768	2331	1572
D	966	706	330
E	1857	1471	1044
Entire region	10 361		6174

4.3.3 Mean Travel Direction

This section discusses the mean direction over the entire lifespan of an eddy. This is the direction from its first day of detection to its last day. Because this section looks at the mean direction over the entire lifespan of eddies, only the long

tracked eddies are used here. There is however no systematic difference in travel direction between short and long-tracked eddies.

Figure 14 shows circular histograms of the travel direction of all regions, also indicating the direction of the RR. South of Iceland in region B eddies travel towards the West, along with the North Atlantic Current which turns below Iceland and flows back South along the Ridge as the East Reykjanes Ridge Current. In Region A2 therefore, the region East of the ridge, eddies still exhibit a strong westward propagation, but they also have a southward component. A lot of eddies in region B will end up in region A2, leading to the strong westward component. If eddies travel towards this region they might travel along the ridge for a few days until they dissolve, leading to minimal impact on the mean travel direction. It is however also possible that some eddies do cross the ridge. Information of the depth of eddies cannot be gained through altimetry data, and mooring observations are not present near the ridge. As the mooring data used in this study shows, eddies do not reach deeper than 850 m, with some eddies only reaching depths of 450 m. It is likely, that some eddies are shallow enough to cross the ridge, while the eddies traveling along the ridge are deeper. On the western side of the ridge (A1) eddies do not show a preferred travel direction. In regions C and E, the central Iceland Basin and Irminger Sea, eddies move mainly towards the west, with minimal meridional movement. In region D, situated within the central region of the Irminger Current, eddies predominantly exhibit northward movement. Furthermore, the distribution of eddies in this region shows an equal representation across different zonal directions, indicating that eddies in region D move northward without a distinct preference for any specific east-west direction. Figure 14d also depicts the direction of eddies obtained from mooring data. These directions align with the directions of the tracked eddies, showing consistency between the two datasets. Overall eddies in the studied region show a strong westward propagation, a feature of eddies ocean wide (Chelton et al., 2007; Chelton et al., 2011), but follow strong ocean currents, such as the East Reykjanes Ridge Current and the Irminger Current, a result also found in other studies (Fu, 2009).

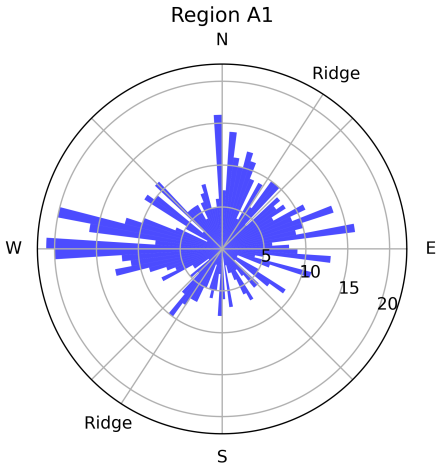

(a) Western flank of RR

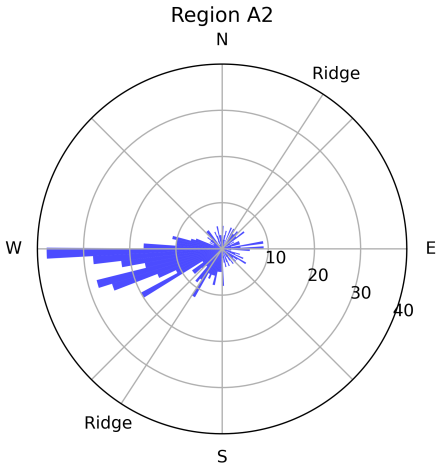

(b) Eastern flank of RR

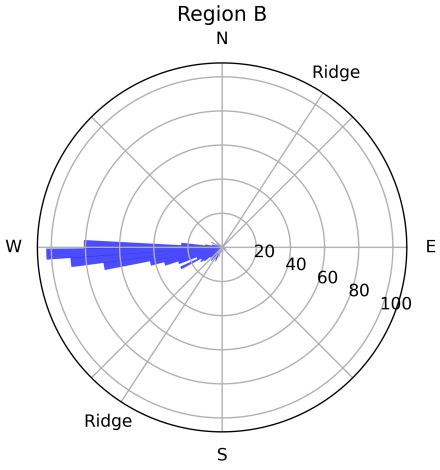

(c) South of Iceland

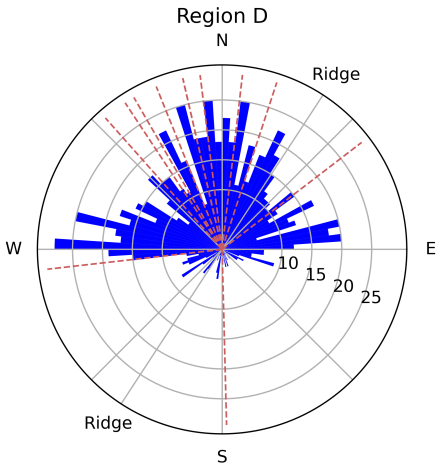

(d) Region around IC1. Red dashed lines show direction of eddies from mooring observations.

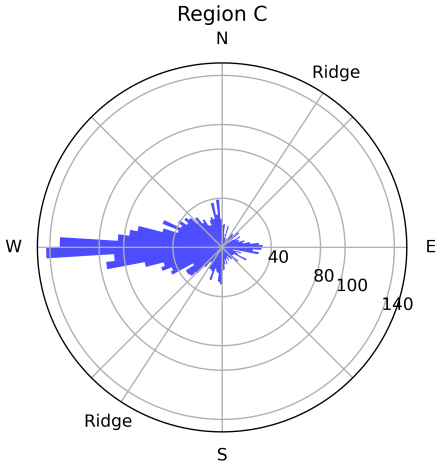

(e) Central Iceland Basin

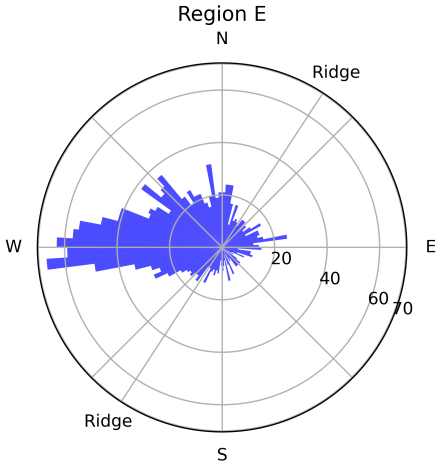

(f) Central Irminger Sea

Figure 14: Histogram of eddy travel direction in different regions. The radial-axis values represent the count of eddies, while the direction of the eddies is indicated from the center outwards. Red dashed lines in region D show direction of eddies from mooring observations.

4.3.4 Influence of background flow on eddy trajectory

This section focuses on examining the day-to-day variations in movement of the projected centers of tracked eddies.

Figure 15a shows the mean geostrophic background velocity from 1993 - 2022. This shows clearly how the geostophic velocity is steered by topography, as well as a strong southward flow at the coast of Greenland, which is where the cold EGC and warmer IC flow southward. Figure 15b shows the eddy velocities from the tracked eddy dataset from 1993 - 2022. The eddy propagation is lower than the background velocity in all parts, except directly South of Iceland, where eddies propagate strictly towards the west, faster than the background flow (North of 61°N and East of -27°E). The gray shaded areas in both Figures indicate the regions where the eddy propagation is directed the same as the background flow. These are the regions with strong currents near shallow topography (the North Atlantic Current, East Reykjanes Ridge Current, Irminger Current, East Greenland Current). In the West, close to Greenland, where strong background velocities are observed, there is a relatively lower presence of eddies, resulting in a limited amount of data available for analysis in this region. However, the available data indicates that the eddies in this area exhibit stronger magnitudes than in all other parts, but eddy propagation is still substantially lower than the background velocity. On the eastern flank of the ridge the eddies also flow with the background, but exhibit higher magnitudes. In Section 4.3.3 we found that eddies do not exhibit a predominant movement along the ridge as their mean travel direction. This shows that eddies reaching the RR originate from diverse locations before traveling along the ridge, which has minimal impact on their overall trajectory. The yellow shaded region shows a strong background flow, but the eddy propagation does not follow it. Instead Figure 15b suggests, that eddies shed off of this current and move westward, showing the generation of eddies due to current instabilities and their strong tendency for westward propagation. Overall eddies therefore follow currents and shallow topography, but in the central parts of the Iceland Basin and Irminger Sea are independent from the background flow.

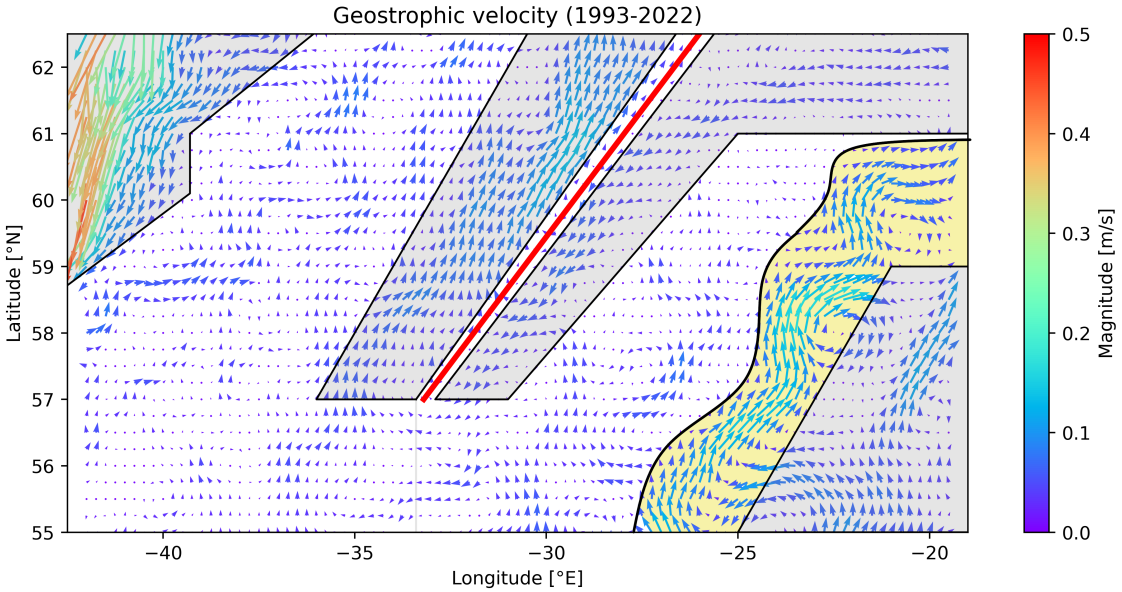

(a) Geostrophic background velocity mean from 1993 - 2022

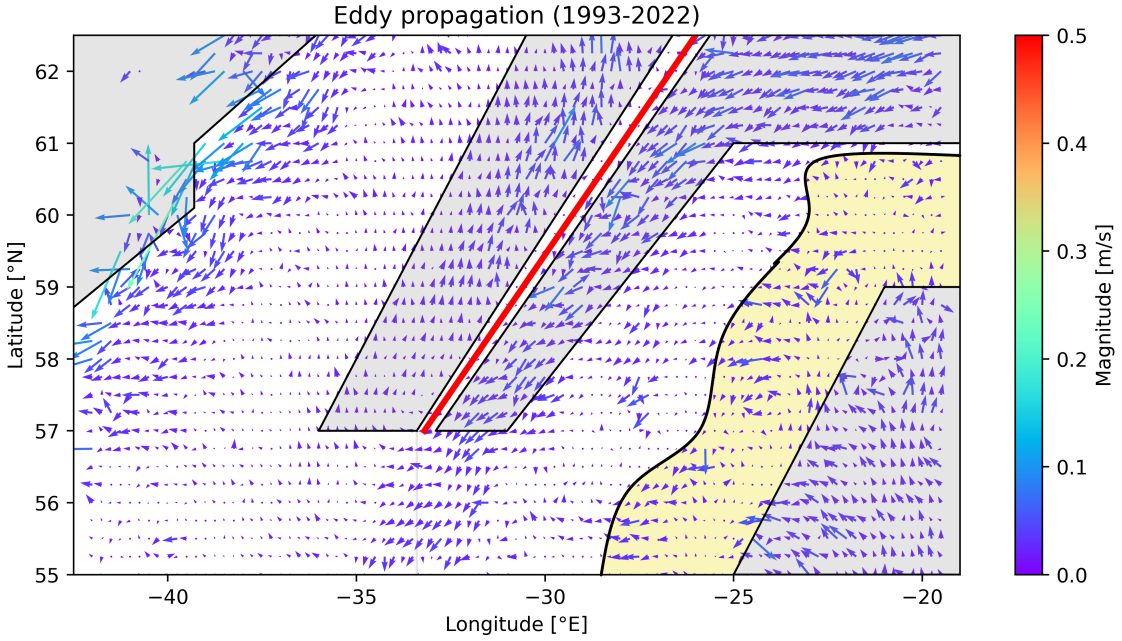

(b) Mean eddy propagation from 1993 - 2022

Figure 15: Mean geostrophic background velocity and mean eddy propagation from 1993 - 2022. Gray shaded areas indicate the regions where eddy propagation follows the background flow. Yellow shaded area highlights a region with strong background flow to the North-East, but westward eddy propagation, showing the generation of eddies from current instabilities and their tendency for westward propagation.

4.3.5 Properties of eddies

Table 4 and 5 present the properties of tracked eddies categorized by region for long and short tracked eddies, respectively. The region does not appear to have a discernible influence on any of the properties, as the values are consistently similar across regions for short and long tracked eddies. The difference in mean size of short and long eddies is quite large, showing, that small-scale eddies have much shorter lifetimes. Long tracked eddies have a mean radius of 34.17 km. The smallest radius of a tracked eddy is 17.1 km, the largest 124 km, though there are only few eddies that have a radius larger than 70 km. Long-tracked eddies exhibit a considerably larger effective radius compared to their speed radius and therefore have a larger effective area. In contrast, short-lived eddies occupy only a small additional space outside their core. The mean duration of long-lived eddies is 60 days. The highest lifetimes of eddies are in region A1 and A2, the regions next to the ridge. West of the ridge eddies do not show a preferred travel direction over their mean lifetime (see Section 4.3.3), the long lifetime and the general tendency of eddies to travel westward however suggest, that eddies are generated near this region and then do not face any strong currents or topography where they potentially dissolve. On the eastern flank of the ridge the long lifetime and mean westward propagation suggest, that eddies travel a long way through the Iceland Basin until they end up near the ridge and dissolve.

In summary, large eddies live much longer than short eddies, showing, that they are more robust. The results also indicate that mesoscale eddies in the Irminger Sea and Iceland Basin are similar to each other in their size, travel direction and the way their propagation is influenced by background flow.

Table 4: Properties of long tracked eddies

Region	Amplitude [cm]	Effective Area [km^2]	Effective Radius [km]	Speed Radius [km]	Duration [days]
A1	4.15	4773	41.16	34.34	60
A2	4.16	4725	41.28	34.63	70
B	4.25	4818	41.35	34.43	63
C	4.18	4739	41.13	34.50	48
D	4.11	4666	40.89	34.41	54
E	4.19	4737	41.10	34.34	46
Entire Region	4.09	4617	40.64	34.17	60

Table 5: Properties of short tracked eddies

Region	Amplitude [cm]	Effective Area [km^2]	Effective Radius [km]	Speed Radius [km]	Duration [days]
A1	1.79	2159	29.81	28.79	5.8
A2	1.81	2252	30.44	29.41	4.1
B	1.88	2197	30.24	29.09	5.7
C	1.76	2195	29.90	28.88	4.3
D	1.80	2264	30.27	29.27	5.5
E	1.76	2221	30.06	29.00	6.7
Entire Region	1.79	2202	29.90	28.87	5.8

5 Conclusions and Outlook

In this study we analyzed mooring observations, sea level anomaly from altimetry data and a global mesoscale eddy trajectory atlas to get a full picture of anticyclonic eddies in the Irminger Sea and Iceland Basin. The primary objective of this study was to quantitatively assess the characteristics of eddies, including the number of eddies, horizontal and vertical structures, and to conduct a comparative analysis of various datasets. The horizontal structures and amount of eddies were primarily assessed using the mesoscale eddy trajectory atlas. In nearly 30 years of observations more than 10 000 eddies have been tracked in this region, with a mean lifetime of 60 days. In a mean over their lifetime they predominantly travel westward, though on a day to day basis eddies follow strong currents near shallow topography, but are otherwise not influenced by background flow. The mean radius of these eddies is around 34 km in the entire region, ranging from 17 km to 70 km, with just some exceptions of larger radii. To assess their vertical structures mooring observations were used. In six years of high resolution mooring observations 12 eddies were detected, though other eddy-like events were also identified. These eddies reach depths between 450 m and 850 m, have a mean salinity of 35.10 g kg^{-1} and a mean temperature of 5.63°C and no systematic changes in salinity and temperature over the 6 years. The radii found from mooring observations range between 16.5 km and 33 km with a mean of 22.7 km. A comparison between the datasets showed, that the eddy trajectory atlas shows similar results as the mooring observations, whereas direct comparison between sea level anomaly from altimetry data and dynamic height anomaly from mooring observations do not agree. This shows the need of a tracking algorithm to robustly assess eddies from altimetry data. 11 out of 12 eddies detected by mooring observations are found in the eddy trajectory atlas. Mooring eddies and the corresponding tracked eddies have the same travel directions, but the tracked eddies have higher radii than mooring eddies. This can be partly because it is more difficult to correctly define the highest velocity of an eddy from altimetry data. Another reason is that in the method used to calculate the radius from mooring data uses the apparent radius. This is half the time it takes for the eddy core to pass the mooring. Most eddies do not pass the mooring directly with the center,

taking less time to cross the mooring,which leads to a shorter apparent radius. de Jong et al., 2014 also found that eddies detected in altimetry data have higher radii than those detected with mooring observations and introduce methods to correct the apparent radius, however in this study we focused on deriving farther characteristics from the eddy trajectory atlas instead of improving the methods to derive characteristics from mooring observations. To study the implications that these anticyclonic eddies have on the deep convection and restratification the amount of eddies that are in the convection zone need to be studied for different years, linking the amount of eddies to the strength of convection and the depth of the mixed layer.

Fan et al., 2013 studied anticyclonic eddies in the Irminger Sea using mooring observations between 2002 - 2009. They found smaller eddies (between 4 km and 21 km) with lower salinity (between 34.97 g kg^{-1} and 35.01 g kg^{-1}) and lower temperature (between 4.2° and 5.3°). The mooring used by Fan et al., 2013 was located specifically to detect eddies in the central Irminger Sea. The location is farther away from the Irminger Current, which can lead to colder and less saline eddies, though it is also possible that eddies have become warmer and more saline over the years. The latter is however not supported by this study that did not find a systematical change of salinity and temperature between 2014 - 2020. Kondetharayil Soman et al., 2022 studied eddies in the Iceland Basin also using the mesoscale eddy trajectory atlas. They used an older version of the atlas that based the tracking on SLA instead of ADT. They only studied eddies with a lifetime longer than 4 weeks and found a mean radius of 60 km. This is larger than the mean radius of 34 km found in this study. The discrepancy can be explained by the fact that they only looked at long lived eddies, which are larger. Though they also used the eddy trajectory atlas an older version can lead to slightly different results, especially if the tracking is not based on the same variable. The difference in radius suggests to further research the difference between eddies in the Iceland Basin and eddies in the Irminger Sea, and to also look at the changes in radius over the lifetime of an eddy.

Mooring observations are important to derive the vertical structure of eddies and determine where the water of eddies comes from. They are also important to evaluate salinity and temperature of eddies and their changes over time. The high

resolution of moorings observations leads to robust estimates of salinity, temperature and depth of eddies. The mooring observations used in this study showed limitation in the extraction of horizontal structures of eddies. These limitations are because the NIOZ moorings locations are not chosen to detect eddies, but to observe the Irminger Current. This leads to large variability in the measured velocities, on which the methods to derive the propagation velocity and radius is based on. Other studies show that the horizontal structures can successfully be derived from moorings at other locations (Lilly and Rhines, 2002; Fan et al., 2013; de Jong et al., 2014). Satellite altimetry can be used to detect and track eddies globally, as has been done with the global mesoscale eddy trajectory atlas. The eddy trajectory atlas enables the quantification of eddies over a large area and the derivation of the horizontal structures. The low temporal and spacial resolution of altimetry data enforces a high rate of interpolation to receive daily data, and therefore the location of eddy properties (center of eddy, contour of maximum speed etc.) are only estimates, especially for eddies that are shorter than 10 days, which is the interval with which satellites pass by the same location. Small scale eddies can therefore not be detected. For a comprehensive understanding of eddies, using more than one dataset is vital.

Some questions regarding mesoscale eddies in the Irminger Sea and Iceland Basin and their impacts remain unresolved. This study focused solely on average values across a 30-year period for all variables. Exploring the interannual variability of eddy activity emerges as a field of study to investigate potential changes in the quantity, size, and propagation of eddies over time. Furthermore, examining changes within an eddy's lifespan, such as whether they progressively decrease in size before they dissolve or first grow over time, presents an additional intriguing aspect. Understanding the origin of water carried by eddies is also crucial. The observed similarities in salinity and temperature from mooring observations in this study suggest that eddies transport water masses of same origins. Another essential step is to conduct similar studies on cyclonic eddies to assess if their behavior and size resemble those of anticyclonic eddies. However, the most important future research endeavor could be establishing a connection between the findings of this study and convection and deep water formation. Investigating the relationship between the amount of eddies in the convection region

and the strength of convection would help evaluate the extent of eddies' impact on restratification. This can be achieved by analyzing convection during different years and examining the presence of eddies during those periods. Evaluating whether the effects of cyclonic and anticyclonic eddies on stratification offset each other becomes an intriguing follow-up question.

6 References

Chelton, D. B., Schlax, M. G., & Samelson, R. M. (2011). Global observations of nonlinear mesoscale eddies. *Progress in Oceanography*, *91*, 167–216. https://doi.org/10.1016/j.pocean.2011.01.002

Chelton, D. B., Schlax, M. G., Samelson, R. M., & de Szoeke, R. A. (2007). Global observations of large oceanic eddies. *Geophysical Research Letters*, *34*(15). https://doi.org/https://doi.org/10.1029/2007GL030812

Danek, C., Scholz, P., & Lohmann, G. (2023). Decadal variability of eddy temperature fluxes in the labrador sea. *Ocean Modelling*, *182*, 102170. https://doi.org/https://doi.org/10.1016/j.ocemod.2023.102170

de Jong, M. F., Bower, A. S., & Furey, H. H. (2014). Two years of observations of warm core anticyclones in the labrador sea and their seasonal cycle in heat and salt stratification. *Journal of Physical Oceanography*, *44*, 427–444. https://doi.org/10.1175/JPO-D-13-070.1

de Jong, M. F., de Steur, L., Fried, N., Bol, R., & Kritsotalakis, S. (2020). Year-round measurements of the irminger current: Variability of a two-core current system observed in 2014–2016 [e2020JC016193 2020JC016193]. *Journal of Geophysical Research: Oceans*, *125*(10), e2020JC016193. https://doi.org/https://doi.org/10.1029/2020JC016193

Delworth, T. L., & Zeng, F. (2012). Multicentennial variability of the atlantic meridional overturning circulation and its climatic influence in a 4000 year simulation of the gfdl cm2.1 climate model. *Geophysical Research Letters*, *39*(13). https://doi.org/https://doi.org/10.1029/2012GL052107

Fan, X., Send, U., Testor, P., Karstensen, J., & Lherminier, P. (2013). Observations of irminger sea anticyclonic eddies. *Journal of Physical Oceanography*, *43*, 805–823. https://doi.org/10.1175/JPO-D-11-0155.1

Fried, N., & de Jong, M. F. (2022). The role of the irminger current in the irminger sea northward transport variability [e2021JC018188 2021JC018188]. *Journal of Geophysical Research: Oceans*, *127*(3), e2021JC018188. https://doi.org/https://doi.org/10.1029/2021JC018188

Fu, L.-L. (2009). Pattern and velocity of propagation of the global ocean eddy variability. *Journal of Geophysical Research: Oceans*, *114*(C11). https://doi.org/https://doi.org/10.1029/2009JC005349

Higginson, S., Thompson, K. R., Huang, J., Véronneau, M., & Wright, D. G. (2011). The mean surface circulation of the north atlantic subpolar gyre: A comparison of estimates derived from new gravity and oceanographic measurements. *Journal of Geophysical Research: Oceans*, *116*(C8). https://doi.org/https://doi.org/10.1029/2010JC006877

Holliday, N. P., Bersch, M., Berx, B., & et al. (2020). Ocean circulation causes the largest freshening event for 120 years in eastern subpolar north atlantic. *Nature Communications*, *11*(1), 585. https://doi.org/10.1038/s41467-020-14474-y

IPCC. (2021). *Climate change 2021: The physical science basis. contribution of working group i to the sixth assessment report of the intergovernmental panel on climate change* (V. Masson-Delmotte, P. Zhai, A. Pirani, S. L. Connors, C. Péan, S. Berger, N. Caud, Y. Chen, L. Goldfarb, M. I. Gomis, M. Huang, K. Leitzell, E. Lonnoy, J. B. R. Matthews, T. K. Maycock, T. Waterfield, Ö. Yelekçi, R. Yu, & B. Zhou, Eds.) [In press]. Cambridge University Press. https://doi.org/10.1017/9781009157896

Jackson, L., Biastoch, A., Buckley, M., Desbruyères, D., Frajka-Williams, E., Moat, B., & Robson, J. (2022). The evolution of the north atlantic meridional overturning circulation since 1980. *Nature Reviews Earth & Environment*, *3*. https://doi.org/10.1038/s43017-022-00263-2

Josey, S. A., de Jong, M. F., Oltmanns, M., Moore, G. K., & Weller, R. A. (2019). Extreme variability in irminger sea winter heat loss revealed by ocean observatories initiative mooring and the era5 reanalysis. *Geophysical Research Letters*, *46*(1), 293–302. https://doi.org/https://doi.org/10.1029/2018GL080956

Kondetharayil Soman, A., Chafik, L., & Nilsson, J. (2022). Linking coherent anticyclonic eddies in the iceland basin to decadal oceanic variability in the subpolar north atlantic [e2021JC018046 2021JC018046]. *Journal of Geophysical Research: Oceans*, *127*(5), e2021JC018046. https://doi.org/https://doi.org/10.1029/2021JC018046

Krauss, W., & Kase, R. H. (1998). Eddy formation in the denmark strait overflow. *Journal of Geophysical Research*, *103*(C8), 15, 525–15, 538. https://doi.org/10.1029/98JC00979

Li, F., Lozier, M. S., Bacon, S., Bower, A., Cunningham, S., de Jong, M., DeYoung, B., Fraser, N., Fried, N., Han, G., et al. (2021). Subpolar north atlantic western boundary density anomalies and the meridional overturning circulation, nat. commun., 12, 3002.

Li, F., Lozier, M. S., Holliday, N. P., Johns, W. E., Le Bras, I. A., Moat, B. I., Cunningham, S. A., & de Jong, M. F. (2021). Observation-based estimates of heat and freshwater exchanges from the subtropical north atlantic to the arctic. *Progress in Oceanography*, *197*, 102640. https://doi.org/https://doi.org/10.1016/j.pocean.2021.102640

Lilly, J. M., & Rhines, P. B. (2002). Coherent eddies in the labrador sea observed from a mooring. *Journal of Physical Oceanography*, *32*, 585–598.

Lozier, M. S., Bacon, S., Bower, A. S., Cunningham, S. A., de Jong, M. F., de Steur, L., deYoung, B., Fischer, J., Gary, S. F., Greenan, B. J. W., Heimbach, P., Holliday, N. P., Houpert, L., Inall, M. E., Johns, W. E., Johnson, H. L., Karstensen, J., Li, F., Lin, X., … Zika, J. D. (2017). Overturning in the subpolar north atlantic program: A new international ocean observing system. *Bulletin of the American Meteorological Society*, *98*(4), 737–752. https://doi.org/https://doi.org/10.1175/BAMS-D-16-0057.1

Marzocchi, A., Hirschi, J. J.-M., Holliday, N. P., Cunningham, S. A., Blaker, A. T., & Coward, A. C. (2015). The north atlantic subpolar circulation in an eddy-resolving global ocean model. *Journal of Marine Systems*, *142*, 126–143. https://doi.org/https://doi.org/10.1016/j.jmarsys.2014.10.007

Mason, E., Pascual, A., & McWilliams, J. (2014). A New Sea Surface Height–Based Code for Oceanic Mesoscale Eddy Tracking. *Journal of Atmospheric and Oceanic Technology*, *31*, 1181–1188. https://doi.org/10.1175/JTECH-D-14-00019.1

Pegliasco, C., Busché, C., & Faugère, Y. (2022). *Mesoscale eddy trajectory atlas meta3.2 delayed-time all satellites: Version meta3.2 dt allsat*. https://doi.org/https://doi.org/10.24400/527896/A01-2022.005.220209

Pegliasco, C., Delepoulle, A., Mason, E., Morrow, R., Faugère, Y., & Dibarboure, G. (2022). META3.1exp: a new global mesoscale eddy trajectory atlas derived from altimetry. *Earth System Science Data*, *14*, 1087–1107. https://doi.org/10.5194/essd-14-1087-2022

Petit, T., Lozier, M. S., Josey, S. A., & Cunningham, S. A. (2020). Atlantic deep water formation occurs primarily in the iceland basin and irminger sea by local buoyancy forcing [e2020GL091028 2020GL091028]. *Geophysical Research Letters*, *47*(22), e2020GL091028. https://doi.org/https://doi.org/10.1029/2020GL091028

Raj, R. P., Johannessen, J. A., Eldevik, T., Nilsen, J. E. Ø., & Halo, I. (2016). Quantifying mesoscale eddies in the lofoten basin. *Journal of Geophysical Research: Oceans*, *121*(7), 4503–4521. https://doi.org/https://doi.org/10.1002/2016JC011637

Sandalyuk, N. V., Bosse, A., & Belonenko, T. V. (2020). The 3-d structure of mesoscale eddies in the lofoten basin of the norwegian sea: A composite analysis from altimetry and in situ data [e2020JC016331 2020JC016331]. *Journal of Geophysical Research: Oceans*, *125*(10), e2020JC016331. https://doi.org/https://doi.org/10.1029/2020JC016331

Sterl, M. F., & de Jong, M. F. (2022). Restratification structure and processes in the irminger sea [e2022JC019126 2022JC019126]. *Journal of Geophysical Research: Oceans*, *127*(12), e2022JC019126. https://doi.org/https://doi.org/10.1029/2022JC019126

Våge, K., Pickart, R. S., Sarafanov, A., Knutsen, Ø., Mercier, H., Lherminier, P., van Aken, H. M., Meincke, J., Quadfasel, D., & Bacon, S. (2011). The irminger gyre: Circulation, convection, and interannual variability. *Deep Sea Research Part I: Oceanographic Research Papers*, *58*(5), 590–614. https://doi.org/https://doi.org/10.1016/j.dsr.2011.03.001

Weaver, A. J., Eby, M., Kienast, M., & Saenko, O. A. (2007). Response of the atlantic meridional overturning circulation to increasing atmospheric co2: Sensitivity to mean climate state. *Geophysical Research Letters*, *34*(5). https://doi.org/https://doi.org/10.1029/2006GL028756

Zhao, J., Bower, A., Yang, J., Lin, X., & Zhou, C. (2018). Structure and formation of anticyclonic eddies in the iceland basin. *Journal of Geophysical Research: Oceans*, *123*(8), 5341–5359. https://doi.org/https://doi.org/10.1029/2018JC013886

Appendices

A Full analysis Eddy 6

Eddy 6 is a shallow eddy that occured in September 2016 at IC1. The full analysis of this eddy is depicted here. Eddy 6 was chosen for various reasons. The velocity signals, as well as temperature and salinity anomalies are not as clear as in other eddies, and therefore this eddy shows the difficulty of extraction from mooring data. In altimetry data and in the eddy trajectory atlas this eddy is nicely visible, and also very long, as is is near the mooring for 29 days and is tracked for 185 days.

Figure 16 shows the Velocity, density, Θ and S signals of the mooring data. Figure 17 shows the vertical profile of the eddy center. In both figure we see that the salinity anomaly is very weak, an generally the salinity is very variable over the duration of the eddy. The temperature anomaly on the other hand is high throughout.

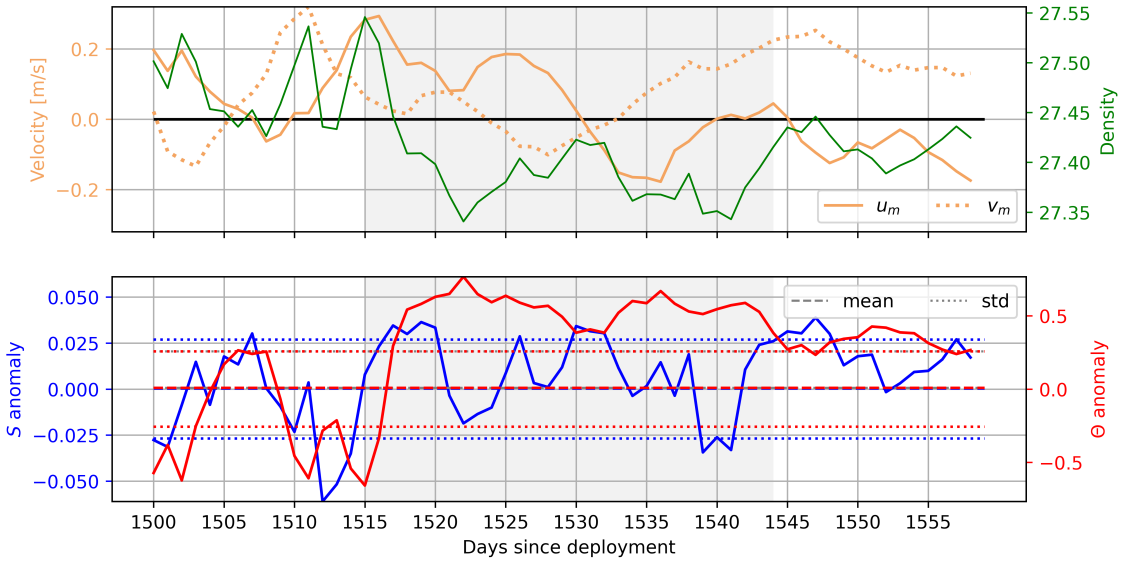

Figure 16: Velocity, density, Θ and S signals of mooring data for Eddy 6. Θ, S and density are the mean over the top 450 m, the velocities are the mean over the top 250 m.

Figure 18 shows the rotated and unrotated velocity signals of eddy six, to best

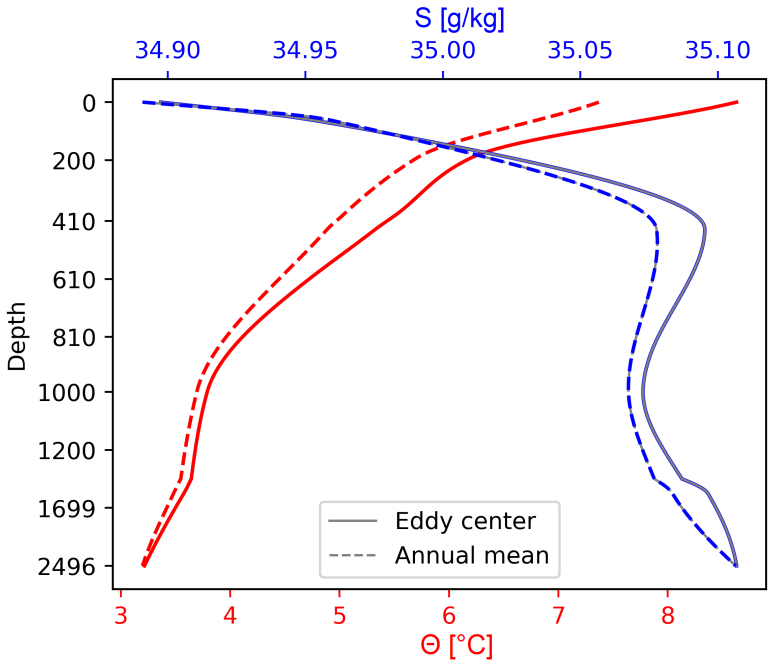

Figure 17: Vertical Θ and S profile of eddy center

fit a Rankine eddy. The rotation angle for this eddy is 3° from North, so the eddy moves northward. Figure 19 shows the fit of the dynamic height gradient to the cross velocity. The fit was only sucessfull on the second edge of the eddy core. The propagation velocity for this eddy using the fit of the second edge is 4.1 cm s^{-1}. The resulting radius is 26.63 km.

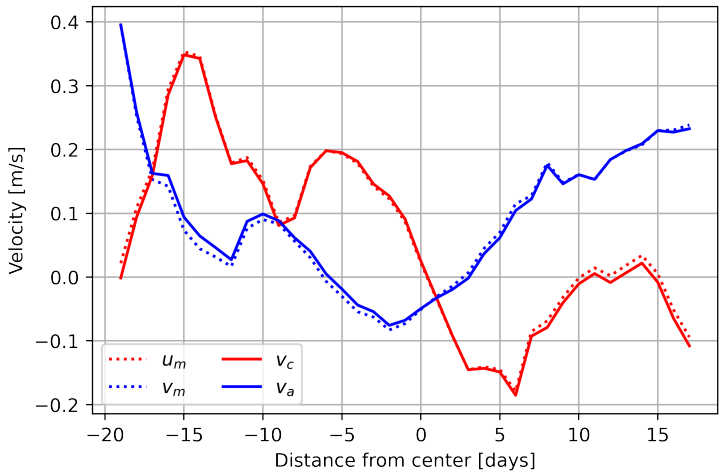

Figure 18: Rotated velocity field to best fit Rankine Eddy. Rotation angle of 3° from N.

In altimetry data the eddy is seen traveling directly across the mooring, and also meandering around the mooring site for quite some time. This lcan also be seen

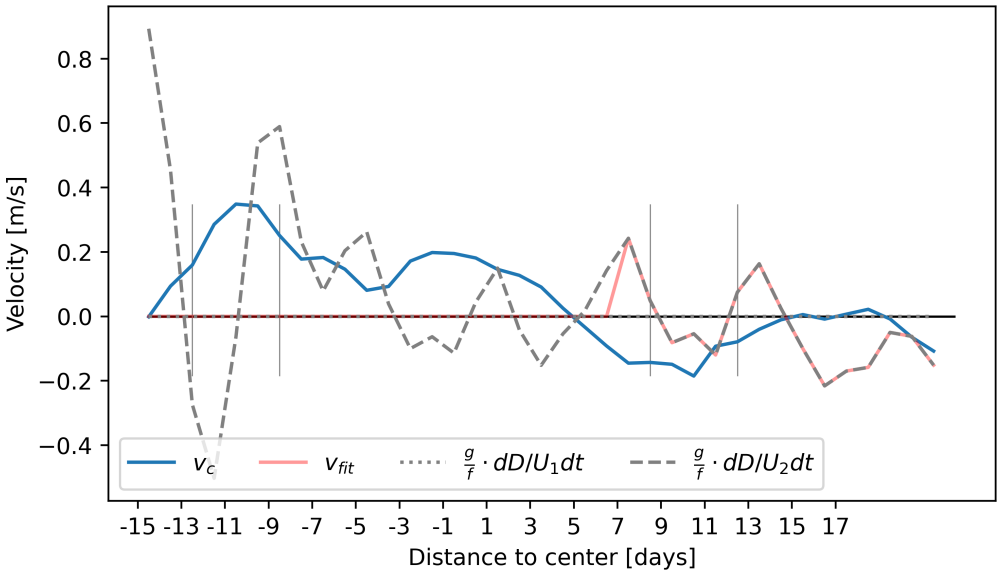

Figure 19: Estimation of propagation velocity by fitting dynamic height gradient the cross velocity v_c. Dotted line presents the fit using the first peak of v_c which is not successful for this eddy. Dashed presents the fit using the second peak (first and second time the eddy core edges cross the mooring).

in the variability of all mooring observations (Θ, S, density and velocities). The direction determined from the mooring data is in accordance with the travel direction seen in altimetry data, though in altimetry data in total the eddy moves not only to the North, but also slightly eastward. While the eddy is near the mooring however, northward movement is seen. Figure 21 shows the entire eddy track. Here we also see, that the eddy is close to the mooring several days and does not move in a straight line, resulting in velocity lines that meander. The eddy core also moves around, resulting in the high variability of Θ and S in the mooring data.

To compare the eddy found in the tracked eddy dataset, we have plotted the loction of the center of the eddy on the ADT map. Black and gray dots indicate the location of the center precious to the current location. Current locations are blue if they are not detected by the eddy, and red if they are detected by the eddy. Adittionally, the green contour shows the radius contour of the eddy, so the location of largest velocities, or the eddy core. The gray contour depicts the effective contour of the eddy, including the outer edges. Figure 22 shows eddy 6 on 4 different days.

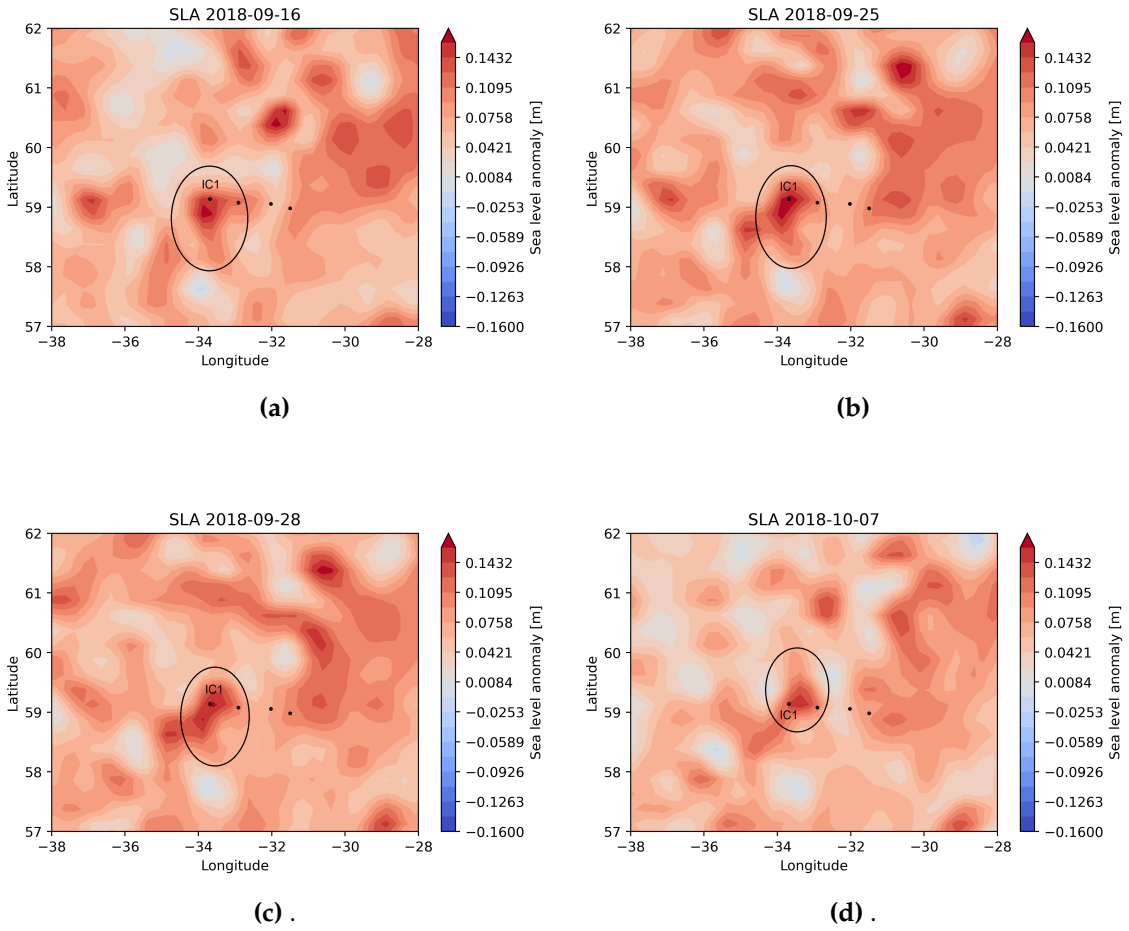

Figure 20: SLA from altimetry data from various days of Eddy 6 in September 2016.

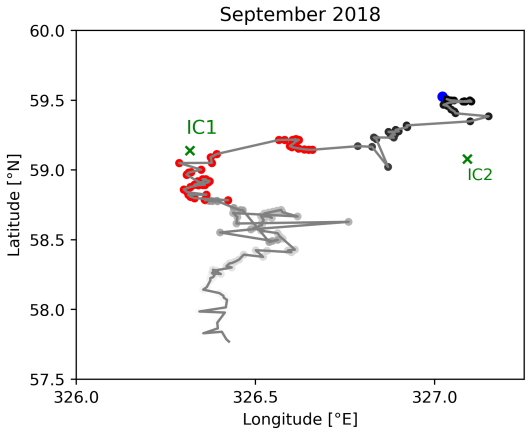

Figure 21: Eddy center of each day eddy 6 was tracked. Time is indicated by color of the line (gray to black). Red dots are the days the eddy was detected in mooring data.

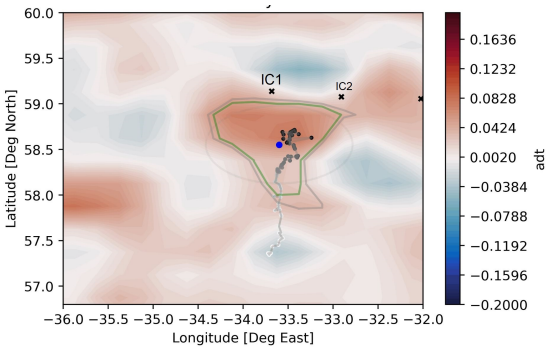

(a) Eddy not yet observed in mooring data

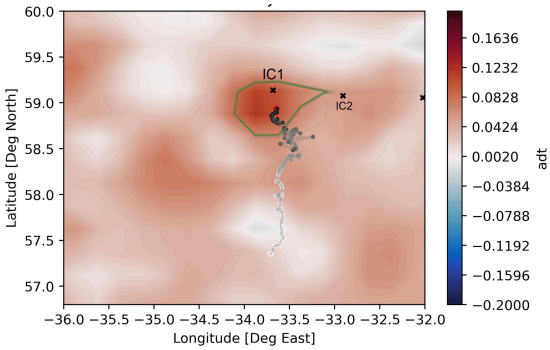

(b) Eddy observed in mooring data

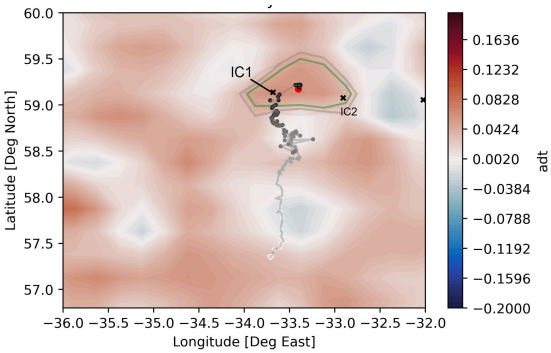

(c) Last day of eddy observed in mooring data

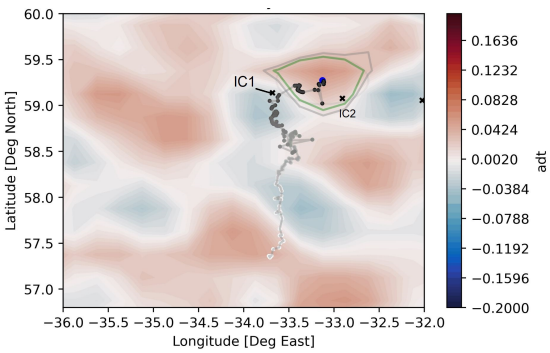

(d) Eddy not observed any more in mooring data

Figure 22: Eddy center. Black and gray are past locations, blue and red are current location where blue dots indicate the eddy is not observed by the mooring, and red dots indicate the eddy is observed by the mooring. Green contour shows the core of the eddy (green line is along highest velocity) and gray line shows the effective contour.